

# Progressive Quantum Algorithm for Quantum Alternating Operator Ansatz

Xiao-Hui Ni,<sup>1,2</sup> Yan-Qi Song,<sup>1</sup> Ling-Xiao Li,<sup>1</sup> Su-Juan Qin,<sup>1,\*</sup> Fei Gao,<sup>1,†</sup> and Qiao-Yan Wen<sup>1</sup>

<sup>1</sup>*State Key Laboratory of Networking and Switching Technology,  
Beijing University of Posts and Telecommunications, Beijing, 100876, China*

<sup>2</sup>*School of Cyberspace Security, Beijing University of Posts and Telecommunications, Beijing, 100876, China*  
(Dated: May 8, 2024)

Recently, Hadfield has proposed a novel Quantum Alternating Operator Ansatz (QAOA+) to tackle Constrained Combinatorial Optimization Problems (CCOPs), and it has wide applications. However, the large requirement of multi-qubit controlled gates in QAOA+ limits its applications in solving larger-scale CCOPs. To mitigate the resources overhead of QAOA+, we introduce an approach termed Progressive Quantum Algorithm (PQA). In this paper, the concept and performance of PQA are introduced focusing on the Maximal Independent Set (MIS) problem. PQA aims to yield the solution of the target graph  $G$  with fewer resources by solving the MIS problem on a desired derived subgraph that has the same MIS solution as  $G$  but has a much smaller graph size. To construct such a desired subgraph, PQA gradually and regularly expands the graph size starting from a well-designed initial subgraph. After each expansion, PQA solves the MIS problem on the current subgraph using QAOA+ and estimates whether the current graph has the same MIS solution as the target graph. PQA repeats the graph expansion and solving process until reaching the stop condition. In our simulations, the performance of PQA is benchmarked on Erdős-Rényi (ER) and regular graphs. The simulation results suggest that PQA showcases higher average approximation ratio (AAR) and significant quantum resource savings compared with directly solves the original problem using QAOA+ (DS-QAOA+) at the same level depth  $p$ . Remarkably, the AAR obtained by PQA is 12.9305% (4.8645%) higher than DS-QAOA+ on ER (regular) graphs, and the average number of multi-qubit gates (qubits) consumed by PQA is  $1/3$  ( $1/2$ ) of that of DS-QAOA+. The remarkable efficiency of PQA makes it possible to solve larger-scale CCOPs on the current quantum devices.

## I. INTRODUCTION

Quantum Approximate Optimization Algorithm (QAOA) [1–5] is a class of hybrid quantum-classical algorithms [6–13] that can be implemented on the current Noisy Intermediate-Scale Quantum (NISQ) devices [14–16] for some small-scale problems. Recently, several researches revolving around QAOA have made certain progress, such as the design of the parameter initialization strategies [17–26] and quantum circuit optimization [27–33]. In addition, the performance of QAOA on solving specific Combinatorial Optimization Problems (COPs) has also been investigated [34–40].

COPs have applications in various fields, including social network analysis, scheduling, and portfolio optimization. The difficulty of solving COPs mainly stems from the exponential growth in the number of possible solutions as the problem size increases. COPs include Constrained Combinatorial Optimization Problems (CCOPs) and Unconstrained Combinatorial Optimization Problems (UCOPs). Compared with UCOPs, solving the CCOPs additionally involves dealing with constraints and validating the feasibility of the output, making it more challenging. Currently, an approach to solving the CCOPs is leveraging Lagrange multiplier to transform CCOP into UCOP [41, 42], where the value of

the introduced penalty term  $\lambda$  is correctly set by many additional hyper-parameter optimization steps [41]. By this operation, the constraints are encoded into a classical objective function that can then be converted into a quantum Hamiltonian whose ground state is the exact solution to the problem. Although QAOA can approximately obtain the ground state by a parameterized quantum circuit (PQC) [38], the Hilbert space includes feasible solutions to the problem as well as terms that violate constraints. Searching for the quasi-optimal solution (i.e., nearly global optimal solution) within an exponential and non-convex space poses a formidable challenge [18]. There is a risk of getting stuck in low-quality local minima during the parameter optimization process [19], obtaining output states that may violate one or more constraints.

To eliminate the nuisance brought by penalty terms in solving CCOPs, Hadfield et al. [28] introduced a novel Quantum Alternating Operator Ansatz (QAOA+) to encode problem constraints into a mixing Hamiltonian  $H_B$ . By this innovation, QAOA+ constructs a subspace that only has feasible quantum states and seeks the solution from it [43]. Hadfield et al. argued that encoding constraints into  $H_B$  (instead of adding penalty terms into the target Hamiltonian) not only limits the size of the search subspace but also improves the average solution quality. So far, QAOA+ has been utilized to tackle many CCOPs and achieves better performance than QAOA [43–48]. However, the implementation of the  $p$ -level QAOA+ ansatz tends to require many multi-qubit con-

\* qsujuan@bupt.edu.cn

† gaof@bupt.edu.cn

trolled quantum gates when solving some CCOPs, where  $p$  is the level depth. Before the execution of QAOA+, these multi-qubit controlled gates must be decomposed into sets of gate operations natively supported by quantum hardware [49]. This high expense hinders the development of QAOA+ on NISQ devices. Searching for heuristic strategies to reduce the consumption of multi-qubit controlled gate in QAOA+, thus effectively utilizing the current limited quantum resources to solve larger-scale CCOPs is a pressing research challenge.

To mitigate the large requirement of quantum resources for QAOA+ ansatz, Saleem et al.[42] proposed Dynamic Quantum Variational Ansatz (DQVA), an approach that increases the number of parameters to be optimized in each level QAOA+ ansatz as done in multi-angle QAOA (ma-QAOA) [5], but DQVA dynamically turns on or off certain parameters to fully utilize the limited quantum resources during optimization. The performance of DQVA is investigated on the maximum independent set (MIS) problem, and the results show the performance of DQVA is improved when each of the partial mixers is given an independent classical parameter. However, the parameter search space exponentially increases with the increase of parameters to be optimized, which further aggravates the difficulty of finding quasi-optimal parameters to a greater extent [18, 26]. Besides, some heuristic strategies aim to reduce the quantum resources by decreasing the size of the optimization problem step by step until the problem becomes trivial to solve [41, 50]. Nevertheless, these strategies typically require abundant expectation function calculations before each reduction of the optimization problem, significantly increasing the additional overhead of the quantum computers. Tomesh et al.[51] presented the Quantum Divide and Conquer Algorithm (QDCA), a method for mapping large COPs onto distributed quantum computers that are achieved via quantum circuit cutting techniques [52]. This technique splits a large quantum circuit into multiple subcircuits that can be independently executed, and then their optimization results are “stitched together” to reconstruct the output of the full circuit. However, the overhead cost of the classical reconstruction step increases exponentially as more cuts are made to the original circuit.

In this paper, **Progressive Quantum Algorithm (PQA)** is proposed to mitigate the costly quantum resource expense when executing the QAOA+ to solve certain CCOPs (whose exact solutions are part of the overall problem). The idea and performance of PQA are introduced by taking the MIS problem as an example. Different from directly solving the problem on the target graph  $G$  like DQVA, PQA aims to iteratively construct a derived subgraph  $G_q$  whose graph size is smaller than the target graph but has the same solution as  $G$ . Naturally, the solution on the target graph can be obtained by solving MIS on the derived subgraph. For the target graph, there may exist multiple derived subgraphs

that have the same MIS solution as  $G$  but with various graph sizes, and the smaller the graph size of the derived graph  $G_q$ , the more resources can be saved. To reduce the consumption of quantum resources as much as possible, the final derived subgraph  $G_q$  is constructed step by step utilizing a well-designed selection rule. After each expansion of graph size, PQA solves the MIS problem on the subgraph using the  $p$ -level QAOA+ ansatz and estimates whether the current subgraph has the same MIS solution as the target graph by comparing the final expectation function values on various subgraphs. In our settings, the circuit parameters are randomly initialized when dealing with the MIS problem on the initial subgraph. Except for it, PQA opts to reuse the pre-trained QAOA parameters corresponding to the previous subgraphs processed by QAOA+ when dealing with the MIS problem on the remaining subgraphs. This operation is referred to as parameter transfer [21, 53–55], a method leverages the observed phenomenon of “parameter concentration” [20, 24].

In our simulations, we benchmark the performance of PQA on multiple Erdős-Rényi (ER) and  $k$ -regular graphs with the number of nodes  $n = 14$ , where  $k = 2, 3$ , and we also give a comparison with the method that directly solves the MIS problem using QAOA+ (DS-QAOA+). Out of all the graphs tested, the simulation results indicate that PQA can achieve an average approximation ratio 12.9305% (4.8645%) higher than DS-QAOA+ on ER ( $k$ -regular) graphs at the same level depth. Furthermore, PQA demonstrates superiority in terms of resource utilization while searching for the optimal solution, consuming on average half the number of qubits compared with DS-QAOA+. Additionally, the average circuit depth of PQA is about 1/3 (2/5) of that of DS-QAOA+ on ER (regular) graphs at the same level depth. More importantly, PQA achieves significant gate savings, conserving approximately 60% (45%) quantum gates (including single RX gate, single RZ gate, and multi-qubit controlled RX gate) compared with DS-QAOA+ on ER (regular) graphs. Particularly, the average number of multi-qubit controlled RX gates consumed by PQA is 1/3 of that of DS-QAOA+. These findings underscore the advantageous computational characteristics of PQA over DS-QAOA+ across a range of graph instances. The remarkable efficiency of PQA makes it possible to solve a larger-scale CCOP on NISQ devices with limited quantum resources today.

This paper is structured as follows: Section II serves as the foundational segment, providing background knowledge on the MIS problem, QAOA, and its extension, QAOA+. Following this, in Section III, we delineate the progressive quantum algorithm, emphasizing the construction rules of the desired derived subgraph. Subsequently, in Section IV, we present a comprehensive set of numerical simulation experiments aimed at showcasing the quantum resource efficiency of PQA over DS-QAOA+. Finally, in Section V, we offer a succinct con-

clusion and discussion to encapsulate the key findings of our study and the next research direction.

## II. PRELIMINARIES

In this section, we introduce some preliminaries to help readers understand our work better.

### A. Review of MIS

MIS is defined in the graph  $G = (V, E)$ , where  $V = \{0, \dots, n-1\}$  is the set of vertices,  $E = \{\{(u, v)\}\}$  is the set of edges, and the two vertices  $u$  and  $v$  on the same edge  $(u, v)$  are adjacent. In this paper, we respectively denote the number of vertices and edges as  $n$  and  $m$ . The vertex subset  $V_s$  is referred to as an independent set of the graph  $G$  if there are no adjacent vertices exist in it. MIS is the vertex subset with the maximum number of vertices among all independent sets. The number of vertices in the MIS is called the independence number, denoted as  $\beta(G)$ . For a graph  $G$ , its solution of MIS is not unique, but the independence number is determined.

For any target graph  $G$ , there exists at least one induced subgraph  $G_q = (V_q, E_q)$  with the same MIS solution as  $G$ , where  $V_q \subseteq V$  and  $E_q \subseteq E$ . Nevertheless, the MIS solution of the target graph may not be the solution of its induced graph. As shown in FIG. 1, FIG 1(b) is the induced graph of FIG 1(a), and they have the same solution of MIS (i.e.,  $\{1, 2, 3\}$ ), but  $\{1, 2, 4\}$  is not the MIS solution of FIG. 1(b) because the node 4 is not in this induced graph. In addition, the independent vertex subsets in  $G_q$  are feasible for  $G$  when  $G_q$  is the induced graph of  $G$ . However, the independent set of  $G$  may not be feasible for  $G_q$ .

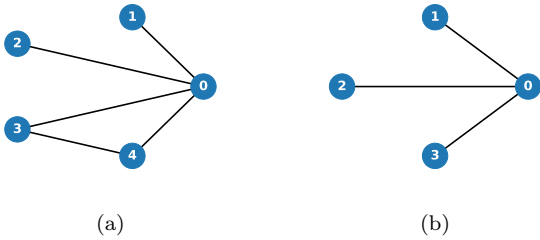


FIG. 1. Examples of MIS. (a) A target graph  $G$  whose feasible solutions are  $\emptyset$ ,  $\{0\}$ ,  $\{1\}$ ,  $\{2\}$ ,  $\{3\}$ ,  $\{4\}$ ,  $\{1, 2\}$ ,  $\{1, 3\}$ ,  $\{1, 4\}$ ,  $\{2, 3\}$ ,  $\{2, 4\}$ ,  $\{1, 2, 3\}$  and  $\{1, 2, 4\}$ . The solutions of MIS are  $\{1, 2, 3\}$  and  $\{1, 2, 4\}$ , where the MIS of  $G$  is not unique, but the independence number identically equals 3. (b) An induced subgraph of  $G$  and its MIS is  $\{1, 2, 3\}$ . The feasible solutions of  $G_q$  are  $\emptyset$ ,  $\{0\}$ ,  $\{1\}$ ,  $\{2\}$ ,  $\{3\}$ ,  $\{1, 2\}$ ,  $\{1, 3\}$ ,  $\{2, 3\}$ ,  $\{1, 2, 3\}$ . We respectively denote the feasible space including all feasible solutions of  $G_q$  and  $G$  as  $S(G_q)$  and  $S(G)$ , where  $S(G_q) \subseteq S(G)$ .

In this paper, we denote  $x_u = 1$  if the vertex  $u$  is in the vertex subset  $V_s$ , otherwise,  $x_u = 0$ , where  $u = 0, 1, \dots, n-1$ . It is straightforward that every way of vertex partition corresponds to a unique bit string  $x$ , and there are  $2^n$  forms for  $x$  in total, where  $x = x_0 x_1 \dots x_{n-1}$ . The goal for MIS is to maximize the objective function

$$C_1(x) = \sum_{u=0}^{n-1} x_u \quad (1)$$

when the constraint  $\sum_{(u,v) \in E} x_u x_v = 0$  is met. The added problem constraint of MIS can be addressed by introducing a Lagrange multiplier into the above objective function [50], thus converting the constrained problem to unconstrained problem whose corresponding classical cost function is

$$\max C(x) = \sum_{u=0}^{n-1} x_u - \lambda \sum_{(u,v) \in E} x_u x_v, \quad (2)$$

where the value of  $\lambda > 1$  can impose penalties on those terms that violate constraints [56], making the MIS solution correspond to the maximal cost function value instead of other feasible or infeasible bit strings. Here,  $C_{max}$  equals the independence number  $\beta(G)$ .

### B. Review of QAOA

Inspired by the quantum adiabatic evolution [57], QAOA encodes the solution of the problem into the ground state of the target Hamiltonian  $H_C$ , and it aims to start from the ground state of the initial Hamiltonian  $H_B$  and gradually evolve to the ground state of  $H_C$  through  $p$ -level QAOA ansatz [1]. For one level QAOA ansatz, it consists of two unitaries  $e^{-i\gamma_i H_C}$  and  $e^{-i\beta_i H_B}$  and two variational QAOA parameters  $\gamma_i$  and  $\beta_i$ , where  $i = 1, 2, \dots, p$  and  $p$  is the level depth. The initial Hamiltonian is conventionally chosen as  $H_B = -\sum_{j=1}^n \sigma_j^x$  whose ground state  $|s\rangle = |+\rangle^{\otimes n}$  can be effective to prepare, where  $\sigma_j^x$  refers that applying Pauli-X to the  $j$ -th qubit. To encode the solution of MIS into the ground state of  $H_C$ , the cost function  $-C(x)$  is converted to the target Hamiltonian

$$H_C = \sum_{u=0}^{n-1} \frac{\sigma_u^z - I}{2} + \lambda \sum_{(u,v) \in E} \frac{I - \sigma_u^z - \sigma_v^z + \sigma_u^z \sigma_v^z}{4} \quad (3)$$

by transforming each binary variable  $x_u$  to a quantum spin  $\frac{I - \sigma_u^z}{2}$  [1], where  $\sigma_u^z$  refers that applying Pauli-Z to the  $u$ -th qubit.

The ground state of  $H_C$  can be approximately obtained by alternately applying unitaries  $e^{-i\gamma_i H_C}$  and  $e^{-i\beta_i H_B}$  on the initial quantum state  $|s\rangle$ . The output state of the

parameterized quantum circuit is

$$|\gamma_{\mathbf{p}}, \beta_{\mathbf{p}}\rangle = e^{-i\beta_{\mathbf{p}}H_B} e^{-i\gamma_{\mathbf{p}}H_C} \dots e^{-i\beta_1 H_B} e^{-i\gamma_1 H_C} |s\rangle, \quad (4)$$

where  $\gamma_{\mathbf{p}} = (\gamma_1, \dots, \gamma_p)$  and  $\beta_{\mathbf{p}} = (\beta_1, \dots, \beta_p)$  are  $2p$  variational QAOA parameters. The expectation value  $F(\gamma_{\mathbf{p}}, \beta_{\mathbf{p}})$  of  $H_C$  in this variational quantum state is defined as

$$F(\gamma_{\mathbf{p}}, \beta_{\mathbf{p}}) = -\langle \gamma_{\mathbf{p}}, \beta_{\mathbf{p}} | H_C | \gamma_{\mathbf{p}}, \beta_{\mathbf{p}} \rangle, \quad (5)$$

which can be calculated by repeated measurements of the output quantum state using the computational basis, and our goal is to search for the global optimal parameters

$$(\gamma_{\mathbf{p}}^{opt}, \beta_{\mathbf{p}}^{opt}) = \arg \max_{(\gamma_{\mathbf{p}}, \beta_{\mathbf{p}})} F(\gamma_{\mathbf{p}}, \beta_{\mathbf{p}}). \quad (6)$$

The search for optimal parameters is typically done by starting with some guesses of the initial parameters, where the quantum computer computes the expectation value of the output state and delivers the relevant information to the classical computer. These parameters are optimized by the classical optimizer and then delivered to the quantum computer. The outer parameter optimization is repeated until it meets the termination condition (e.g., the maximal number of iterations or convergence tolerance  $\varepsilon$  [26]). To quantify the quality of the QAOA solution (i.e., measure the difference between the output state of QAOA and the ground state of  $H_C$ ), we introduce the approximation ratio (AR)

$$r = \frac{F(\gamma_{\mathbf{p}}, \beta_{\mathbf{p}})}{F_{max}}, \quad (7)$$

where  $F_{max}$  is the negative of the ground state energy of  $H_C$ . Here,  $F_{max}$  equals the independence number of the graph which can be obtained by brute force search for small graph instances. For large graphs, we can execute multiple runs of greedy algorithm [58] and utilize the maximal vertices number among the obtained independent set to approximate  $F_{max}$ . AR reflects how close the solution provided by QAOA is to the true solution,  $r \leq 1$ , with the value of 1 is the true solution.

### C. Review of QAOA+

The Lagrange multiplier method searches for the ground state in a Hilbert space, encompassing a broader set of quantum states that may not adhere to the independence constraint, potentially resulting in output states that violate constraints [39, 41]. To address this limitation, Hadfield et al. [28, 43] introduce a novel quantum alternating operator denoted as QAOA+.

Different from adding the constraints into the target Hamiltonian utilizing the penalty term, QAOA+ encodes the constraints into the mixer Hamiltonian. By this operation, QAOA constructs a subspace that only comprises

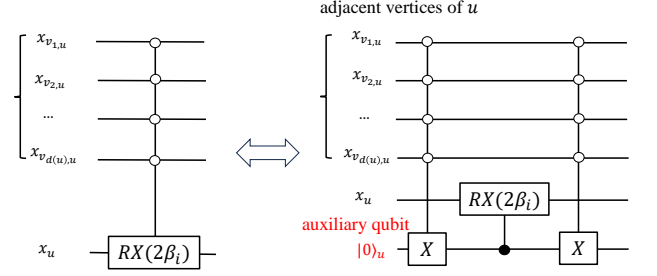


FIG. 2. The quantum circuit of  $e^{-i\beta_i B_u}$  can be implemented by two multi-qubit controlled gates, a single-qubit controlled RX gate, and an auxiliary qubit. The auxiliary qubit transfers from  $|0\rangle$  to  $|1\rangle$  only when the quantum states of all adjacent vertices are  $|0\rangle$ , then a single qubit rotation RX operation is executed on the  $u$ -th qubit. Otherwise, there is an Identify operation applied to the  $u$ -th qubit when the auxiliary qubit is always  $|0\rangle$ . The right multi-qubit controlled gate operation can reset the state of the auxiliary qubit from  $|1\rangle$  to  $|0\rangle$  when there is a flip in the previous operation.

the single and the superposition of feasible states, and aims to search for the optimal solution from it. At this time, the corresponding target Hamiltonian

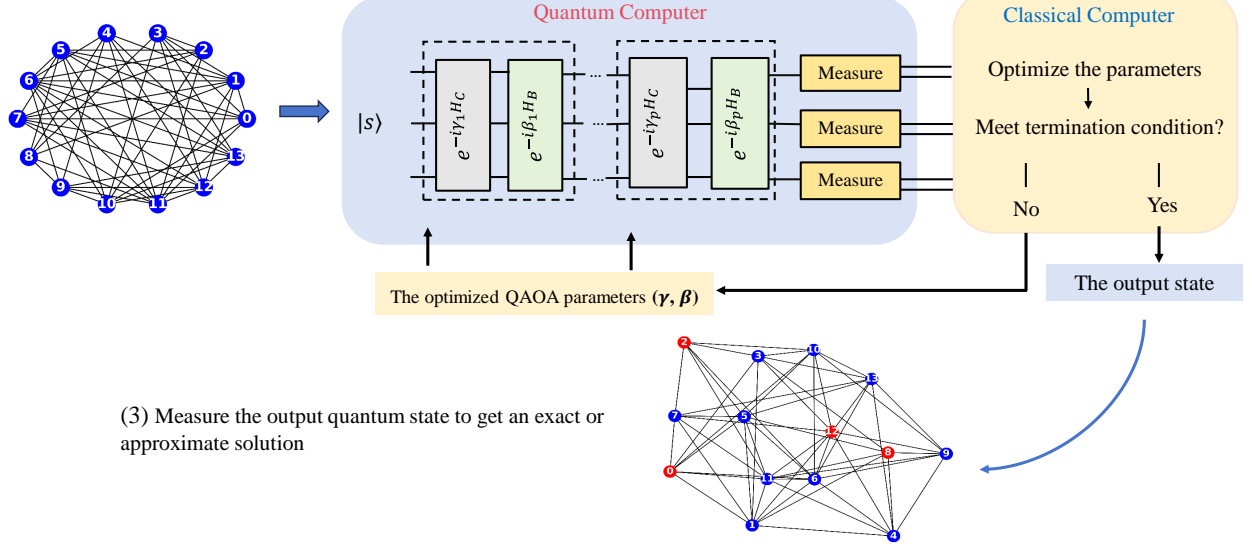
$$H_C = \sum_{u=0}^{n-1} \frac{\sigma_u^z - I}{2} \quad (8)$$

is obtained by converting the  $x_u$  in  $-C_1(x)$  to a quantum spin  $\frac{I - \sigma_u^z}{2}$ , encoding the MIS solution into the ground state of  $H_C$ . Similar to QAOA, QAOA+ approaches the ground state of  $H_C$  by alternately applying unitaries  $e^{-i\gamma_i H_C}$  and  $e^{-i\beta_i H_B}$  on the initial quantum state  $|s\rangle$ . However, the initial quantum state in QAOA+ must be a single feasible state or the superposition of feasible states to keep the feasible space. In addition,  $|s\rangle$  may not be the ground state of  $H_B$  in QAOA+, which is also different from the original QAOA.

The design of  $H_B$  must keep (i.e., ensure the space has no states violating the constraints) and explore the feasible space (i.e., provide transitions between various feasible states). For an independent vertex subset  $V_s$ , deleting any vertices from  $V_s$  does not change its independence. However, a new vertex  $v_a$  can be added into  $V_s$  without destroying the independence of  $V_s$  only when its all adjacent vertices are not in  $V_s$ , these above rules can be described as

$$f(v_a) = \sum_{j=1}^{d(v_a)} x_{v_{j,a}} = 0, \quad (9)$$

where  $v_{j,a}$  and  $d(v_a)$  respectively represent the  $j$ -th adjacent vertex of  $v_a$  and the number of adjacent vertices of  $v_a$ . Here, the subscript  $j = 1, \dots, d(v_a)$ , and the new vertex  $v_a$  can not be added into  $V_s$  when  $f(v_a) > 0$ . Mapping to a quantum circuit, for any vertex  $u$ , a Pauli-

(1) Input the target graph  $G$  to be solved(2) Build the PQC according to  $G$  and execute optimization

(3) Measure the output quantum state to get an exact or approximate solution

FIG. 3. A schematic of directly solving the MIS problem on the target graph using QAOA or QAOA+ ansatz, where the choice of the initial quantum state  $|s\rangle$ , the mixer Hamiltonian  $H_B$ , and the target Hamiltonian  $H_C$  are relevant to the choice of ansatz.

X operation is applied on the  $u$ -th qubit if and only if all the states of adjacent vertices of  $u$  are  $|0\rangle$  (i.e.,  $f(u) = 0$ ). Otherwise, it is equivalent to performing a Pauli-I operation on the  $u$ -th qubit. For any vertices  $u \in V$ , the mixer rules that conjointly implement the operations of deleting and adding nodes from the independent vertex subset can be described as

$$B_u = \sum_{f(u)=0} |x_{v_1,u} \cdots x_{v_{d(u),u}}\rangle \langle x_{v_1,u} \cdots x_{v_{d(u),u}}| \otimes \sigma_u^x + \sum_{f(u)>0} |x_{v_1,u} \cdots x_{v_{d(u),u}}\rangle \langle x_{v_1,u} \cdots x_{v_{d(u),u}}| \otimes I. \quad (10)$$

The mixer Hamiltonian  $H_B = \sum_{u=0}^{n-1} B_u$ , where the state obtained by applying  $e^{-i\beta_i B_u}$  on the single feasible quantum state  $|x_o\rangle$  is

$$e^{-i\beta_i B_u} |x_o\rangle = \begin{cases} \cos 2\beta_i |x_o\rangle - i \sin 2\beta_i |x_0 \cdots \bar{x}_u \cdots x_{n-1}\rangle, \\ |x_o\rangle, f(u) > 0, \end{cases} \quad (11)$$

where the  $\bar{x}_u$  denotes the state of the node  $u$  is converted from  $|0\rangle$  ( $|1\rangle$ ) to  $|1\rangle$  ( $|0\rangle$ ), implementing the operation of adding or deleting vertices without changing the independence. The above Eq. 11 suggests that the mixer operator can keep the feasible space and provide the transition among different feasible states (i.e., the operation of adding and deleting nodes). The corresponding quantum circuit of  $e^{-i\beta_i B_u}$  is shown in FIG. 2, and Table I is provided to more intuitively show the differences between QAOA and QAOA+ when solving the MIS problem. In addition, we also give a schematic to depict the process

of directly solving the MIS problem on the target graph using the QAOA or QAOA+ ansatz in FIG. 3 to help readers understand our subsequent work better.

### III. PROGRESSIVE QUANTUM ALGORITHM

For a target graph  $G$ , its derived subgraph whose number of vertices is  $\beta(G)$  and the number of edges is zero is the MIS solution of  $G$ , and it has the strongest sparsity (i.e., the number of edges is much less than the number of nodes) among all induced subgraphs. However, it is NP-Hard to find such a derived subgraph. In this paper, PQA retreats and aims to iteratively construct a sparse and small-scale (i.e., the number of nodes is small) derived subgraph that has the same MIS solution as the target graph starting from an initial subgraph, and we refer to this subgraph as “desired induced subgraph”. Naturally, the solution of the target graph can be obtained with fewer resources by solving the MIS problem on the desired subgraph compared with directly solving. The fundamental steps of PQA are as follows: PQA starts with a sparse and small-scale initial induced subgraph  $G_0$ , and the MIS problem on  $G_0$  is solved using  $p$ -level QAOA+ ansatz. Then, PQA gradually expands this subgraph using the well-designed rules. After each expansion, PQA retrains the circuit using pre-trained parameters to solve the MIS problem on the newly induced subgraph. Repeat the above expansion and solving procedures until reaching the termination condition.

In the realization of  $e^{-i\gamma_i H_B}$  and  $e^{-i\gamma_i H_C}$  based on the structure of  $G_q$ , fewer quantum gates and qubits are required as the number of nodes and edges of the desired

TABLE I. The difference between QAOA and QAOA+ when solving the MIS problem

	QAOA	QAOA+
Manipulation of constraints	Encode it into $H_C$	Encode it into $H_B$
Initial state $ s\rangle$	$ s\rangle =  +\rangle^{\otimes n}$	The single or superposition of feasible states
Mixer Hamiltonian $H_B$	$H_B = -\sum_{u=0}^{n-1} \sigma_u^x$	$H_B = \sum_{u=0}^{n-1} B_u$
Target Hamiltonian $H_C$	$H_C = \sum_{u=0}^{n-1} \frac{\sigma_u^z - I}{2} + \lambda \sum_{(u,v) \in E} \frac{I - \sigma_u^z - \sigma_v^z + \sigma_u^z \sigma_v^z}{4}$	$H_C = \sum_{u=0}^{n-1} \frac{\sigma_u^z - I}{2}$
$ s\rangle$ is the ground state of $H_B$ ?	Yes	No requirement
Hilbert space	Including feasible and infeasible states	Feasible states

graph  $G_q$  decrease. However, there may be multiple derived subgraphs of different graph sizes that have the same MIS as the target graph, further impacting the number of quantum gates and qubits required in a parametric quantum circuit. Constructing a small-scale induced subgraph with the same MIS solution as the target graph is one of the key points of PQA. In the following, the construction rules of the desired induced subgraph and how to estimate whether the induced subgraph has the same MIS solution as the target graph are introduced.

#### A. The construction rules of the subgraph

To construct such a sparse desired induced subgraph, the subgraph is gradually expanded from a sparse and small-sized initial subgraph, while the graph expansion process prefers the inclusion of the points with the lowest “closeness” to the current subgraph to maintain the graph structure (especially, the sparsity of graph). The closeness is measured by a classical objective function

$$C(v_c) = \sum_{v_c \in V_c, v_q \in V_q} E(v_c, v_q), \quad (12)$$

where the vertex candidate set  $V_c = V - V_q$  and  $V_q$  is the vertex set of the current induced subgraph  $G_q$ . If the nodes  $v_c$  and  $v_q$  are adjacent (i.e.,  $(v_c, v_q) \in E$ ),  $E(v_c, v_q) = 1$ . Otherwise,  $E(v_c, v_q) = 0$ . The value of  $C(v_c)$  measures the effect of the addition of vertex  $v_c$  to the current induced subgraph  $G_q$  on the sparsity of the induced graph, and a small value of  $C(v_c)$  indicates that there is a slight change in the sparsity of the induced subgraph if the node  $v_c$  is added to  $G_q$ . In our construction rules, the vertices that have the least effect on sparsity are preferred to be added to the currently derived subgraph to minimize the effect of the new node on sparsity.

The key points of the construction of the initial subgraph with  $n_0$  nodes are the choice of the first node and the selection of the newly added nodes. The detailed selection rules are as follows:

**The choice of the first node.** To construct a sparse

initial subgraph  $G_0$ , the node with a minimal degree in the target graph  $G$  is chosen as the first node of  $G_0$ . If there are  $l(> 1)$  nodes with the minimal degree, we randomly choose one as the first node.

**The extension of subgraph.** The addition of new nodes should have as little effect on the graph sparsity as possible. We opt for the node with  $\min C(v_c)$  from the candidate set as the next vertex to join the current subgraph. If there are  $l(> 1)$  nodes with  $\min C(v_c)$ , we conduct the next round of calculation. We suppose the node with  $\min C(v_c)$  is added to the current subgraph and respectively calculate the next value of  $\min C(v_c)$ , and we can get  $l$  calculation results. The node that corresponds to  $\min(\min C(v_c))$  is chosen as the next node. If there are multiple nodes with  $\min(\min C(v_c))$ , we randomly choose one as the next node. If the newly added node  $v_{new}$  is adjacent to the other nodes in the current subgraph, the corresponding edges should be supplemented with the current subgraph. Then, repeat the process of extension until we get a subgraph with  $n_0$  nodes.

In conclusion, the extension of the subgraph includes the addition of new nodes and edges. The node with the lowest correlation with the nodes in the current subgraph is preferred to be added to ensure the sparsity of the graph. To help readers understand the above rules, we give an example in **Appendix A**.

#### B. Progressive quantum optimization

After constructing an initial induced subgraph  $G_0$ , PQA builds a parameterized quantum circuit using the  $p$ -level QAOA+ ansatz to solve the MIS problem on  $G_0$ , where the parameters are randomly initialized. After optimization, PQA continues to expand the graph size (obeying the same selection rules as the extension of the initial subgraph), and the corresponding  $p$ -level QAOA+ ansatz based on the new subgraph is constructed to solve the MIS problem on it. The PQC reuses the optimized QAOA parameters from the previous subgraph and re-optimizes these pre-trained parameters. This operation is referred to as “parameter transfer” [53, 54], a method leverages “parameter concentration” (i.e., for

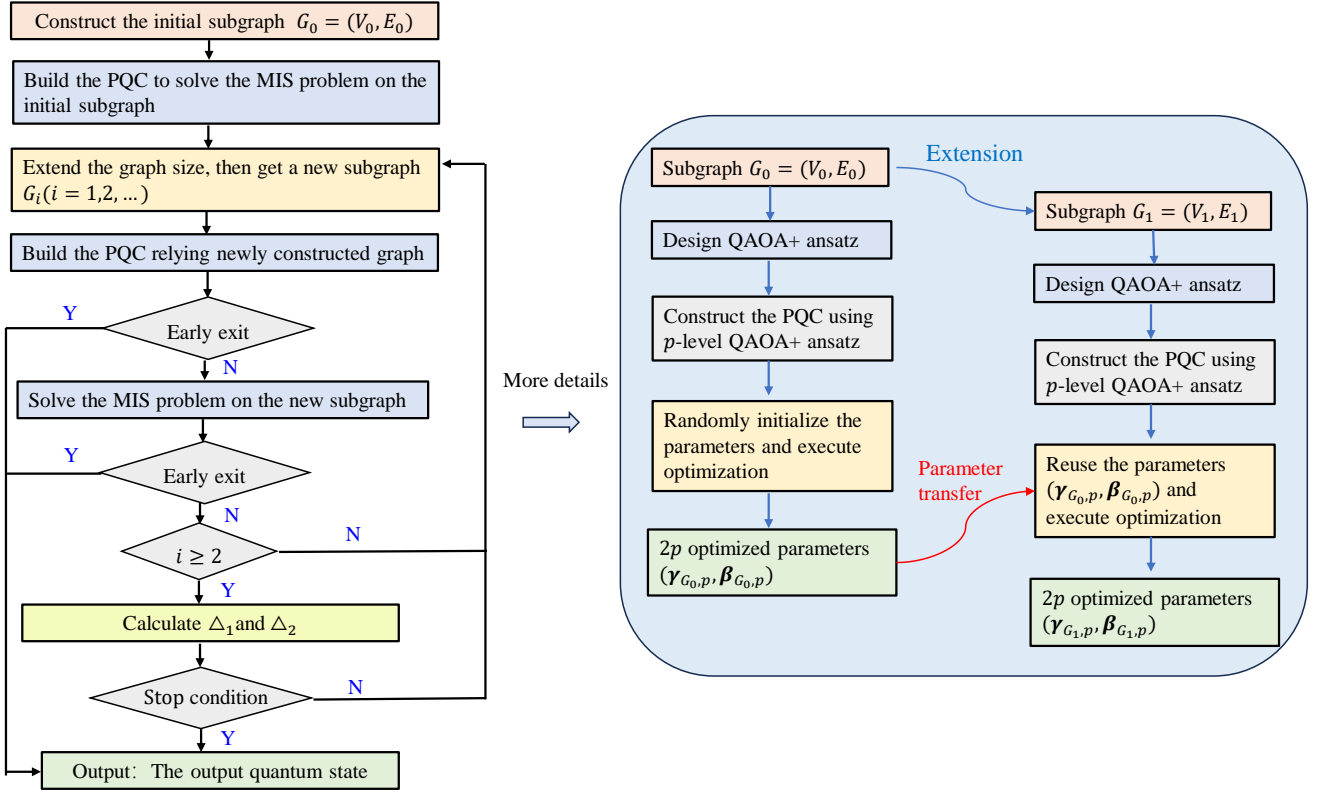


FIG. 4. A procedure schematic for PQA. The basic steps of PQA are as follows: PQA starts by solving the MIS problem on the initially induced subgraph  $G_0$  using  $p$ -level QAOA+ ansatz, where the parameters are randomly initialized. Subsequently, PQA gradually extends the graph size, and then the MIS problem on the current subgraph is solved by using the corresponding  $p$ -level QAOA+ ansatz, where the PQC is retrained by reusing the pre-trained parameters. After optimization, PQA estimates whether the current subgraph has the same MIS solution as the target graph by comparing the obtained function values on various subgraphs. In particular, PQA introduces two early exit mechanisms to avoid the waste of quantum resources. The first (second) mechanism is to judge the necessity of executing this optimization (the subsequent extension of the graph). When PQA does not meet the first mechanism, the PQC outputs the quantum state on the subgraph  $G_{i-1}$  ( $G_i$  represents the newly constructed subgraph). The output state that corresponds to the maximal  $F_{G_j,p}$  ( $j = 0, 1, \dots, i$ ) is given when PQA does not meet the second mechanism. Except for the above two cases, the output quantum state is obtained on the subgraph  $G_i$  when PQA satisfies the stop condition.

these graphs are with similar graph structure, the optimal parameters on a small-scale graph can still show good performance when migrated to a larger-scale graph) [20, 24]. After each optimization round, PQA can get a relevant expectation function value. In our setting, PQA is terminated if the obtained values satisfy  $\Delta_1 \leq \xi$  and  $\Delta_2 \leq \xi$  or obtaining the same size as the target graph in the worst case, where

$$\begin{aligned} \Delta_1 &= |F_{G_{i+1},p} - F_{G_i,p}|, \\ \Delta_2 &= |F_{G_i,p} - F_{G_{i-1},p}|. \end{aligned} \quad (13)$$

Here,  $\xi$  is the tolerance on function values and  $F_{G_i,p}$  ( $F_{G_{i-1},p}$ ) represents the obtained function value when using  $p$ -level QAOA+ ansatz to solve the MIS problem on the current (previous) subgraph  $G_i$  ( $G_{i-1}$ ).

In this paragraph, we explain why  $\Delta_1 \leq \xi$  and  $\Delta_2 \leq \xi$  are the termination conditions. Adding a new vertex to the current sparse derived subgraph  $G_i$  may make the corresponding maximal expectation values and the inde-

pendence number increase or unchanged (i.e.,  $F_{max,G_i} \leq F_{max,G_{i+1}}$  and  $\beta(G_i) \leq \beta(G_{i+1})$ ). When PQA starts with a subgraph that has the same MIS solution as the target graph, there will be no growth in the corresponding maximal expected function values  $F_{max,G_i}$  as the continuous escalation of the subgraph size (i.e.,  $F_{max,G_i}$  reaches a steady state). Nevertheless, it is also possible that the value of  $F_{max,G_i}$  will continue to ascend with the increase of the graph size after a brief period of stagnation when PQA starts with other initial subgraphs. During the transient stationary phase, the addition of new nodes does not yield added benefits (i.e., without incrementing the maximal expectation function value), and this situation is due to getting trapped in a “local subgraph”, which is affected by the ill-fitting node selection. For the latter case, the subsequent enlargement of the graph might enhance returns, but it concurrently requires more quantum resources to construct the corresponding quantum circuits. At this time, scaling the graph size without regard to resources is not advisable,

and PQA is required to cut loss in time. Motivated by both cases, we prioritize the stable phase of change in the expected function value during optimization, and PQA is halted if the value of the expected function remains relatively constant across three consecutive expansion iterations. At this juncture, we may have discovered a derived subgraph with the same MIS solution as the target graph, or we may have attained an approximate solution by solving the MIS problem on the local subgraph.

The above idea about the stop condition in Eq. 13 is proposed based on the ideal situation that the maximum expected value  $F_{max, G_i}$  can be obtained on each subgraph. However, the quality of the reused parameters can affect the optimization result in each subgraph. During the actual optimization, the expected function value may oscillate back and forth with the increase in graph size when the effect of parameter transfer is ill, delaying in meeting the stop condition, such as shown in **Appendix B**. In this situation, PQA may not satisfy the termination condition and continue to execute optimization until reaching the same scale as the target graph, even though a subgraph with the same solution as the target graph has been constructed, which is contrary to the original intention of PQA. To reduce the consumption of running costs in a run of PQA, on one hand, we try to improve the quality of reused parameters by a greedy operation as done in Ref. [23, 59] when solving the MIS problem of  $G_0$ . Detailedly, we can execute  $c$  rounds of optimization when PQA solves the MIS problem on the initial induced subgraph, then select one set of the optimized parameters that correspond to the maximal function value in  $c$  sets of results. The preserved parameters are reused to solve the MIS problem on the next subgraph. On the other hand, it is necessary to set up some early exit mechanisms to end the low-cost optimization, and this idea is implemented from the judge of the quality of the reused parameters and the optimization results in each subgraph. After each graph extension, we first determine whether this optimization round is executed by judging the quality of the reused (initial) parameters. When PQA starts with high-quality initial parameters, PQA can converge to quasi-optima after a few iterations (or even no optimization). Otherwise, it may require abundant iterations to reach convergence or get stuck in a low-quality local solution. Therefore, we terminate PQA in advance and do not execute this round of optimization if the expected function value corresponding to the initial parameter under this circuit is significantly lower than that obtained by optimization on the above subgraph. If the quality of the initial parameters meets the rules we set, a new round of early exit judgments will be carried out after the optimization. When the latest expected function value is significantly lower than the maximal function value obtained in the previous few subgraphs, indicating that the optimization has fallen into a poor local solution. PQA will not carry out the subsequent expansion of the graph scale and optimization, and return the maximal function value in this run and

corresponding output state. Otherwise, PQA continues to execute if it satisfies the above settings. All in all, to reduce the resources required in a run of PQA, we introduced two early exit mechanisms that determines the necessity of executing the following optimization rounds by the ‘flags’ (the quality of the initial parameters and the optimization results). PQA cannot get the optimal solution to the problem through an optimization run as DS-QAOA+, and it simply aims to solve the problem with as few quantum resources as possible. More detailed procedures of PQA are shown in FIG. 4.

PQA is a hybrid quantum-classical algorithm, where the concept of hybrid quantum-classical encompasses two aspects. Firstly, when using the QAOA+ algorithm to solve the MIS problem on a subgraph, the classical computer handles parameter optimization while the quantum computer computes the expected function value. This constitutes an external parameter optimization loop, achieving synergy between classical and quantum computation. Secondly, in constructing the subgraph, the classical computer constructs a new subgraph based on the structural information of the target graph, while the quantum computer executes the MIS problem-solving on the subgraph and determines the classical computer whether it needs to continue expanding the subgraph based on the optimization results, which constitutes another collaborative process. In summary, PQA leverages the parallel computing capabilities of the quantum computer to solve the MIS problem on each subgraph, while sharing the a part of costs (such as obtaining target graph information and parameter adjustment) with the classical computer, instead of undertaking all overheads of resources by quantum or classical computers.

#### IV. NUMERICAL SIMULATIONS

In our work, the effects of graph construction rules and the initial graph size  $n_0$  on the performance of PQA are firstly investigated. Taking the graph shown in FIG. 5 as an example, the detailed investigation results are introduced as follows.

##### A. The effects of graph construction rules and $n_0$ on the performance of PQA

On the given graph instance, we respectively conduct  $100 \times p$  runs of PQA following various graph construction rules, where  $n_0 = 1$ ,  $\xi = 0.1$ , and the quantum state  $|s\rangle$  is initialized as  $|0\rangle$  at each solving process. Subsequently, we calculate the AR obtained by PQA at level  $p = 1$  when it follows different construction rules. Notably, the AR is the ratio between the expectation function value obtained by PQA on the final induced subgraph and  $F_{max, G}$ , where  $F_{max, G}$  denotes the maximal expectation function value on the target graph, equivalent to the independence number of the target graph.

The AR is less than or equal to 1, with an exact ratio of 1, signifying that PQA has successfully achieved the MIS solution of the target graph by solving the MIS problem on the current subgraph.

Our simulation results show that PQA can get the exact solution at  $p = 1$  when it starts from an arbitrary first node and randomly expands the subgraph during the optimization. However, the AAR obtained by PQA is the lowest in this situation, as shown in FIG. 6, PQA can achieve a higher AAR when it expands the subgraph by rules. Given these phenomena, we analyze in detail the variation of the expected function value with the size of the subgraph, and we find that the parameter transfer will show poor performance when the addition of random vertices causes a large change in the graph structure, resulting in early termination of the optimization run. This situation is because the obvious changes in the graph structure cause a large change in the function landscape, at this time, the transferred parameters may be low-quality parameters for the new landscape. Nevertheless, our designed graph expansion rules maintain the graph structure well while maintaining the sparsity of the graph, making better use of the parameter transfer strategy and exhibiting good performance. Additionally, FIG. 7 provides the total number of iterations consumed by PQA under various construction rules while achieving the exact solution. These findings indicate that PQA requires fewer iterations to obtain the optimal solution when following our graph construction rules, resulting in a significant reduction of 95.486% of iterations compared with random first node and expansion (i.e., ‘NN’). In summary, the results presented in FIG. 6 and FIG. 7 collectively demonstrate the efficiency of our proposed graph construction rules.

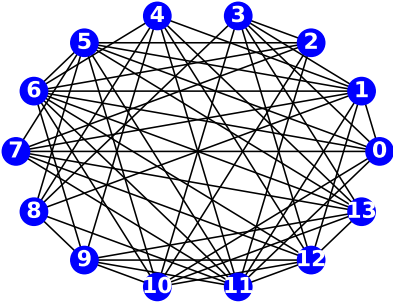


FIG. 5. An ER random graph with  $n = 14$ ,  $m = 55$ , and prob = 0.4. The MIS solution of this graph obtained by 1000 runs of the greedy algorithm is  $\{0, 2, 8, 12\}$  and  $\{0, 2, 8, 13\}$ . Thus, the independence number and  $F_{max,G}$  equal 4.

Furthermore, we also explore the impact of  $n_0$  on the performance of PQA under various  $p$ . In our simula-

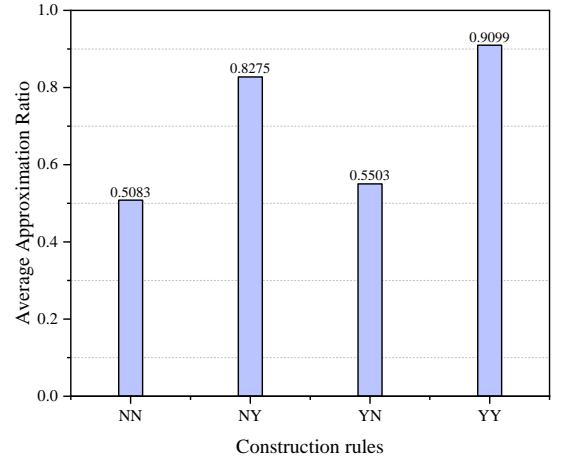


FIG. 6. The effects of graph construction rules on the AAR obtained by PQA, where ‘NN’ suggests PQA arbitrarily chooses the first node and subsequent nodes without any rules. ‘NY’ represents that the first node is randomly chosen, while other newly added nodes obey our predetermined expansion rules.

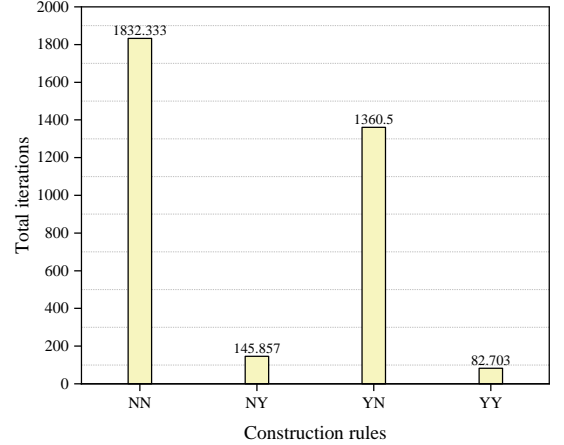


FIG. 7. The effects of graph construction rules on the total consumption of iterations to get the exact MIS solution.

tions, we set the level depth from one to five, and execute  $100 \times p$  runs of PQA at each level depth. The resulting AR versus the level depth and  $n_0$  is depicted in FIG. 8. These simulation results suggest that PQA can get the exact MIS solution (i.e., OAR = 1) at  $p = 1$  when it starts from initial subgraphs with  $n_0 = 2, 4, 6$ . Nevertheless, PQA requires more level depths to get the exact solution when the size of the initial problem to be solved is large. Concretely, the level depth consumed by PQA with  $n_0 = 14$  (i.e., DS-QAOA+) is at least 5, and the corresponding consumption of circuit depth and quantum gates are 215 and 140 (including 70 multi-qubit controlled RX gates and 70 RZ gates). While for PQA with  $n_0 = 2, 4$ , its expenditure of the circuit depth and quantum gates are 15 and 12 when getting the quasi-optima, respectively saving 93% and 91.4% of resources compared with DS-QAOA+. More details of the require-

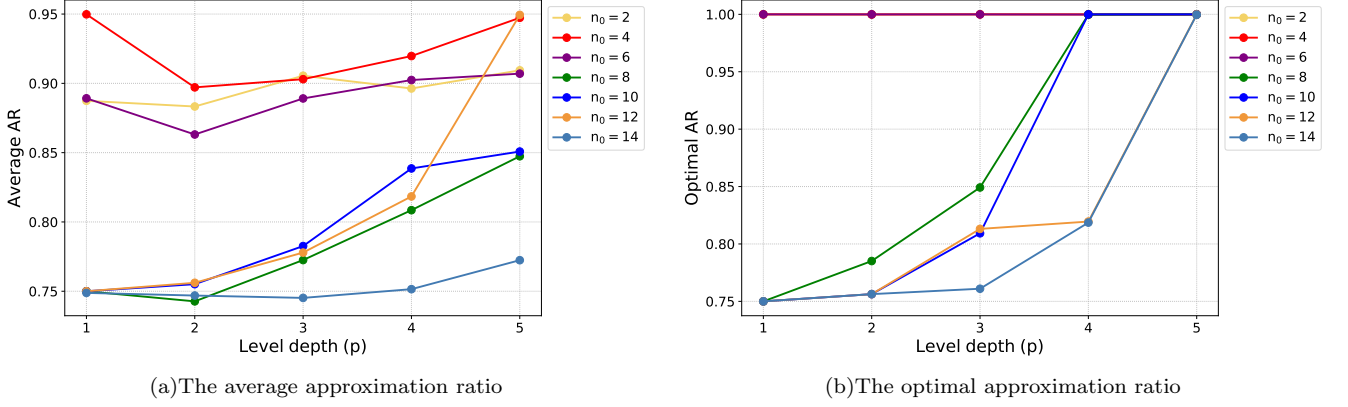


FIG. 8. The AR obtained by PQA under various level depths  $p$  and  $n_0$ , where  $n_0$  is the number of nodes of the initial induced subgraph  $G_0$ . Each solid dot in the curve reflects the AR obtained by PQA at level depth  $p$  when it starts from a subgraph with  $n_0$ . Specifically, the curve reflects the AR of DS-QAOA+ under various level depths when  $n_0 = 14$ . (a) The obtained AAR of PQA. The results show that PQA requires more level depths to get a larger AAR when  $n_0$  is too large. (b) The obtained OAR of PQA. The results show that PQA can get the exact solution (i.e., OAR equals one) at  $p = 1$  when it starts from an induced subgraph with  $n_0 = 2, 4, 6, 8$ . However, the level depths consumed by DS-QAOA+ is at least 5 to achieve the MIS solution.

TABLE II. The average consumption of PQA versus level depth and  $n_0$ .

$n_0$	$p = 1$			$p = 2$			$p = 3$			$p = 4$			$p = 5$		
	q	d	g	q	d	g	q	d	g	q	d	g	q	d	g
2	6	15	2,6,4	5	28	2,10,8	4	27	6,12,6	7	88	0,28,28	6	75	10,30,20
4	6	15	2,6,4	5	20	6,10,4	6	51	3,18,15	6	68	4,24,20	6	85	5,30,25
6	8	25	1,8,7	8	50	0,16,16	8	75	0,24,24	8	100	0,32,32	8	115	5,40,35
8	10	31	0,10,10	9	56	0,18,18	9	84	0,27,27	10	124	0,40,40	10	155	0,50,50
10	12	37	0,12,12	12	74	0,24,24	12	111	0,36,36	10	124	0,40,40	12	185	0,60,60
12	14	43	0,14,14	14	86	0,28,28	14	129	0,42,42	14	172	0,56,56	13	200	0,65,65
14	14	43	0,14,14	14	86	0,28,28	14	129	0,42,42	14	172	0,56,56	14	215	0,70,70

ments of quantum resources of PQA (with different  $n_0$ ) at various  $p$  are given in Table II, where the average consumption of qubits, the circuit depth, and the number of quantum gates (RX, RZ, multi-qubit controlled RX) in an optimization run of PQA are simply denoted as q, d, and g. These results demonstrate an optimization run of PQA tends to consume more resources when it starts from a large-scale induced subgraph.

In addition, the total consumption of iterations and optimization runs are also investigated when PQA initializes from various  $n_0$  and gets the exact MIS solution, as given in FIG. 9. These findings elucidate the increasing demand for iterations and optimization runs to reach the optimal solution as  $n_0$  exceeds a certain threshold. Moreover, our analysis reveals substantial efficiency gains with PQA, with savings of at least 92% in iterations and 95% in runs compared with DS-QAOA+ for attaining the MIS solution. The total quantum resources are determined by multiplying the average consumption per run by the total number of runs necessary to achieve a quasi-optimal solution. FIG. 10 provides a comprehensive overview of the

total consumption of quantum resources as PQA initializes from various  $n_0$  values and achieves a quasi-optimal solution. Notably, PQA achieves quasi-optimal solutions while consuming only 3.867% of the quantum resources required by DS-QAOA+. Underscoring its potential for resource-efficient optimization, these efficiency gains are particularly significant given the current limitations of available quantum resources.

Our investigation emphasizes the sensitivity of PQA to the choice of  $n_0$ . There may be a potential decline in its performance when PQA initializes with a large-scale initial subgraph. To maintain robust performance in subsequent simulations, we opt for  $n_0 = 2$ . This decision is informed by our observation that smaller values of  $n_0$  tend to yield more reliable results, ensuring the stability and effectiveness of PQA across varied scenarios. Nevertheless, the choice of  $n_0$  remains a pivotal aspect for future exploration, as it holds the potential to further reduce the number optimization rounds in a run under other initialization options, enhancing the efficiency of

TABLE III. The average consumption of an optimization run of PQA and DS-QAOA+ on ER graphs.

Types	No.	Algorithm	$p = 1$			$p = 2$			$p = 3$			$p = 4$			$p = 5$		
			q	d	g	q	d	g	q	d	g	q	d	g	q	d	g
ER, prob = 0.4	G1	PQA	6	15	2,6,4	5	28	2,10,8	4	27	6,12,6	7	88	0,28,28	6	75	10,30,20
		DS-QAOA+	14	43	0,14,14	14	86	0,28,28	14	129	0,42,42	14	172	0,56,56	14	215	0,70,70
	G2	PQA	5	14	1,5,4	5	20	6,10,4	6	51	3,18,15	4	36	8,16,8	6	85	5,30,25
		DS-QAOA+	14	43	0,14,14	14	86	0,28,28	14	129	0,42,42	14	172	0,56,56	14	215	0,70,70
	G3	PQA	6	17	1,6,5	7	44	0,14,14	7	66	0,21,21	6	68	4,24,20	5	70	5,25,20
		DS-QAOA+	14	43	0,14,14	14	86	0,28,28	14	129	0,42,42	14	172	0,56,56	14	215	0,70,70
	G4	PQA	5	14	1,5,4	5	28	20,10,8	4	24	6,12,6	5	56	4,20,16	4	45	10,20,10
		DS-QAOA+	14	43	0,14,14	14	86	0,28,28	14	129	0,42,42	14	172	0,56,56	14	215	0,70,70
	G5	PQA	6	15	2,6,4	5	20	6,10,4	5	30	9,15,6	5	40	12,20,8	5	70	5,25,20
		DS-QAOA+	14	43	0,14,14	14	86	0,28,28	14	129	0,42,42	14	172	0,56,56	14	215	0,70,70
ER, prob = 0.5	G1	PQA	7	18	2,7,5	7	32	6,14,8	5	36	6,15,9	6	52	12,24,12	6	65	15,30,15
		DS-QAOA+	14	43	0,14,14	14	86	0,28,28	14	129	0,42,42	14	172	0,56,56	14	215	0,70,70
	G2	PQA	7	22	0,7,7	6	38	0,12,12	5	42	3,15,12	7	88	0,28,28	7	110	0,35,35
		DS-QAOA+	14	43	0,14,14	14	86	0,28,28	14	129	0,42,42	14	172	0,56,56	14	215	0,70,70
	G3	PQA	6	15	2,4,6	5	20	6,10,4	6	45	6,18,12	5	48	8,20,12	6	75	10,30,20
		DS-QAOA+	14	43	0,14,14	14	86	0,28,28	14	129	0,42,42	14	172	0,56,56	14	215	0,70,70
	G4	PQA	6	15	2,6,4	6	30	4,12,8	5	42	3,15,12	6	60	8,24,16	4	45	10,20,10
		DS-QAOA+	14	43	0,14,14	14	86	0,28,28	14	129	0,42,42	14	172	0,56,56	14	215	0,70,70
	G5	PQA	6	15	2,6,4	5	20	6,10,4	8	69	3,24,21	5	40	12,20,8	6	75	10,30,20
		DS-QAOA+	14	43	0,14,14	14	86	0,28,28	14	129	0,42,42	14	172	0,56,56	14	215	0,70,70

TABLE IV. The average consumption of an optimization run of PQA and DS-QAOA+ on regular graphs.

Types	No.	Algorithm	$p = 1$			$p = 2$			$p = 3$			$p = 4$			$p = 5$		
			q	d	g	q	d	g	q	d	g	q	d	g	q	d	g
2-regular graph	G1	PQA	9	22	3,9,6	8	34	8,16,8	9	66	9,27,18	9	80	16,36,20	8	85	20,40,20
		DS-QAOA+	14	43	0,14,14	14	86	0,28,28	14	129	0,42,42	14	172	0,56,56	14	215	0,70,70
	G2	PQA	8	15	5,8,3	8	34	8,16,8	8	51	12,24,12	8	60	20,32,12	8	85	20,40,20
		DS-QAOA+	14	43	0,14,14	14	86	0,28,28	14	129	0,42,42	14	172	0,56,56	14	215	0,70,70
	G3	PQA	8	17	4,8,4	8	34	8,16,8	8	51	12,24,12	8	68	16,32,16	9	110	15,45,30
		DS-QAOA+	14	43	0,14,14	14	86	0,28,28	14	129	0,42,42	14	172	0,56,56	14	215	0,70,70
	G4	PQA	8	15	5,8,3	10	54	4,20,16	9	66	9,27,18	8	68	16,32,16	9	110	15,45,30
		DS-QAOA+	14	43	0,14,14	14	86	0,28,28	14	129	0,42,42	14	172	0,56,56	14	215	0,70,70
	G5	PQA	8	17	4,8,4	8	34	8,16,8	8	51	12,24,12	8	68	16,32,16	8	85	20,40,20
		DS-QAOA+	14	43	0,14,14	14	86	0,28,28	14	129	0,42,42	14	172	0,56,56	14	215	0,70,70
3-regular graph	G1	PQA	7	14	4,7,3	5	20	6,10,4	7	48	9,21,12	6	44	16,24,8	7	80	15,35,20
		DS-QAOA+	14	43	0,14,14	14	86	0,28,28	14	129	0,42,42	14	172	0,56,56	14	215	0,70,70
	G2	PQA	7	16	3,7,4	7	32	6,14,8	7	48	9,21,12	7	64	12,28,16	7	80	15,35,20
		DS-QAOA+	14	43	0,14,14	14	86	0,28,28	14	129	0,42,42	14	172	0,56,56	14	215	0,70,70
	G3	PQA	6	15	2,6,4	8	34	8,16,8	7	36	15,21,6	7	48	20,28,8	9	110	15,45,30
		DS-QAOA+	14	43	0,14,14	14	86	0,28,28	14	129	0,42,42	14	172	0,56,56	14	215	0,70,70
	G4	PQA	8	19	3,8,5	8	38	6,16,10	7	48	9,21,12	7	64	12,28,16	7	80	15,35,20
		DS-QAOA+	14	43	0,14,14	14	86	0,28,28	14	129	0,42,42	14	172	0,56,56	14	215	0,70,70
	G5	PQA	8	21	2,8,6	7	32	6,14,8	6	33	12,18,16	7	64	12,28,16	8	105	10,40,30
		DS-QAOA+	14	43	0,14,14	14	86	0,28,28	14	129	0,42,42	14	172	0,56,56	14	215	0,70,70

TABLE V. The total consumption of quantum resources when PQA and DS-QAOA+ obtain the quasi-optimal solution by multiple optimization runs.

Types	No.	DS-QAOA+			PQA		
		q	d	g	q	d	g
ER, prob = 0.4	G1	1400	21500	0,7000,7000	10.908	27.27	3.636,10.908,7.272
	G2	700	10750	0,3500,3500	29.09	81.452	5.818,29.09,23.272
	G3	3921.568	168627.424	0,82913.512,82913.512	7.998	22.661	1.333,7.998,6.665
	G4	25.452	78.174	0,25.452,25.452	5	14	1,5,4
	G5	1400	43000	0,14000,14000	7.5	18.75	2.5,7.5,5
	Mean	1489.404	48791.1196	0,21487.7928,21487.7928	12.0992	32.8266	2.8574,12.0992,9.2418
ER, prob = 0.5	G1	14285.712	438775.44	0,142857.12,142857.12	12.726	14.544	3.636,12.726,9.09
	G2	14285.712	438775.44	0,142857.12,142857.12	10.003	31.438	0,10.003,10.003
	G3	700	10750	0,3500,3500	7.5	18.75	2.5,5,7.5
	G4	4778.158	146757.71	0,47781.58,47781.58	7.998	19.995	2.666,7.998,5.332
	G5	1400	21500	0,7000,7000	10.908	27.27	3.636,10.908,7.272
	Mean	7089.9164	211311.718	0,68799.164,68799.164	9.827	22.3994	2.4876,9.327,7.8394
2-regular	G1	14285.712	438775.44	0,142857.12,142857.12	90	220	30,90,60
	G2	14285.712	438775.44	0,142857.12,142857.12	17.776	33.33	11.11,17.776,6.666
	G3	23.338	358.405	0,116.69,116.69	8	17	4,8,4
	G4	14285.712	438775.44	0,142857.12,142857.12	17.776	33.33	11.11,17.776,6.666
	G5	21.56	331.1	0,107.8,107.8	8.88	18.87	4.44,8.88,4.44
	Mean	8580.4068	263403.165	0,85759.17,85759.17	28.4864	64.506	12.132,28.4864,16.3544
3-regular	G1	14285.712	438775.44	0,142857.12,142857.12	28	56	16,28,12
	G2	14285.712	438775.44	0,142857.12,142857.12	14	320	60,14,80
	G3	46.662	143.319	0,46.662,46.662	10.002	25.005	3.334,10.002,6.668
	G4	7179.494	220513.03	0,71794.94,71794.94	32	76	12,32,20
	G5	14285.712	438775.44	0,142857.12,142857.12	22.856	59.997	5.714,22.8556,17.142
	Mean	10016.6584	307396.5338	0,100082.5924,100082.5924	21.3716	107.4004	19.4096,21.37152,27.162

PQA across diverse problem instances.

### B. The performance comparison between PQA and DS-QAOA+

In our simulations, we randomly generate five graphs for different ER graphs (with prob = 0.4, 0.5) and  $k$ -regular graphs ( $k = 2, 3$ ) with the number of nodes  $n = 14$ . Subsequently, we benchmarked the performance of PQA and DS-QAOA+ on these graphs. On each graph instance, we independently execute  $100 \times p$  runs of DS-QAOA+ and PQA at level depth  $p$ , where the tolerance on function values  $\xi = 0.1$  and the quantum state  $|s\rangle$  is initialized as  $|0\rangle$  at each solving process. In each optimization round to solve the MIS problem on subgraph, the classical outer parameter optimization loop is ended if the convergence tolerance [26] satisfies  $\varepsilon \leq 0.001$ .

We plot the AR obtained by PQA and DS-QAOA+ on the given graphs. From our examples in FIG. 11, we observe that PQA outperforms DS-QAOA+ with an average approximation ratio higher by 12.9305% (4.8645%) on ER ( $k$ -regular) graphs at the same level depth. Remarkably, PQA achieves the exact MIS solution at a shallow depth  $p = 1$  for all tested graph instances, whereas DS-QAOA+ at least requires  $5 \times p$  level depths to achieve a similar performance, as observed in 80% of the tested graphs. Besides, the numerical simulation results in FIG. 11 indicate that PQA achieves varying average approximation ratios at the same level depth when solving MIS problems on different graphs. Apart from the influence of initial parameters, we speculate that this discrepancy is also related to the graph structure. For certain graphs, the random selection of vertices during the graph expansion process may lead PQA to easily fall into “local subgraphs”, causing premature termination of the

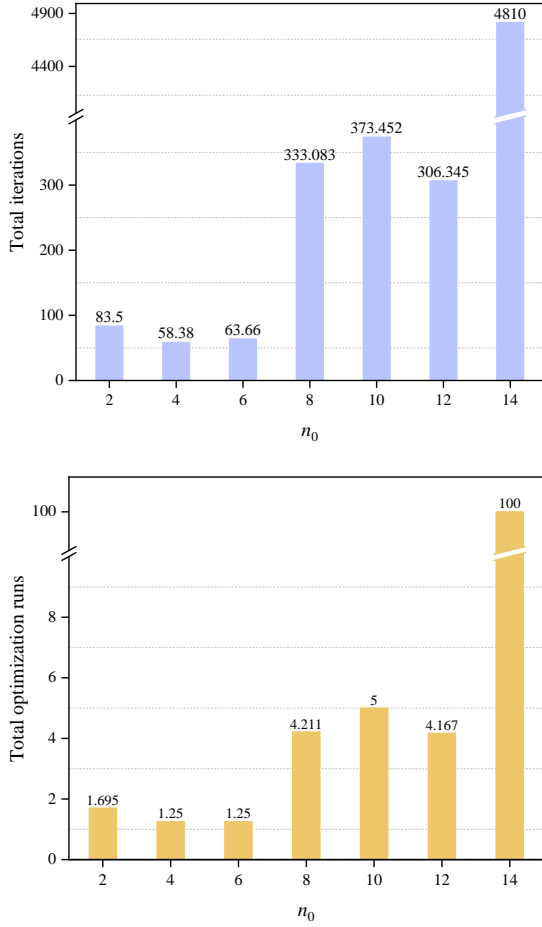


FIG. 9. The total consumption of iteration and optimization runs when PQA starts from the initial subgraphs with  $n_0$  and gets the exact MIS solution.

optimization process. We analyzed the numerical optimization results of PQA when solving MIS problems on ER graphs (with prob = 0.5) 4 and graph 5, and found that in solving the MIS problem on graph 5, PQA sometimes terminates during the optimization due to falling into local subgraphs (but similar situations occur to a lesser extent in graph 4), resulting in an expected function value lower than  $F_{max,G}$ . Similar situations also occur in 2-regular graph 1, 3-regular graph 1, and graph 5. These cases further confirm our hypothesis.

Additionally, we provide Table III and Table IV to compare the average quantum resources consumption of PQA and DS-QAOA+ at the same level depth. Specifically, PQA consumes, on average, half the number of qubits compared with DS-QAOA+. Moreover, the average circuit depth of PQA is approximately 1/3 (2/5) that of DS-QAOA+ on ER (regular) graphs. Notably, PQA achieves significant gate savings, conserving approximately 60% (45%) of quantum gates (including single RX gate, single RZ gate, and multi-qubit controlled RX gate) compared with DS-QAOA+ on ER (regular) graphs. Particularly noteworthy is that the average num-

ber of multi-qubit controlled RX gates consumed by PQA is only 1/3 of that by DS-QAOA+. Incorporating with FIG. 11, we observe that **PQA can not only obtain a higher average approximation ratio but also consume far fewer quantum resources than DS-QAOA+ under the same level depth**. These findings highlight the superior resource utilization capabilities of PQA, enabling the solution of larger-scale CCOPs on NISQ devices with limited quantum resources.

In the external parameter optimization loop, each iteration needs multiple calls of the quantum processing units (QPUs) to calculate the expectation function value. More iterations mean more requirements of the QPUs, resulting in more consumption of the quantum resources. To reflect the performance of PQA and DS-QAOA+ from different aspects, we also calculate the total consumption of iterations and optimization runs of PQA and DS-QAOA+ when they achieve the quasi-optimal solution. In our work, for those graph instances where DS-QAOA+ can not get the quasi-optimal solution at  $5 \times p$ , we additionally set level depth from 5 to  $n$  and execute multiple optimization runs at level depth  $p$  to search for a similar quasi-optimal solution to PQA. We compare the total optimization runs and iterations consumed by PQA and DS-QAOA+ when they get the quasi-optima, and more details are shown in FIG. 12. These results show that PQA can get the quasi-optima while consuming 1.357% (1.188%) of the iterations (runs) required by DS-QAOA+ on ER graphs with prob=0.4. On ER graphs with prob=0.5, the iterations and runs of PQA are respectively 2.1% and 3.02% of the consumption of DS-QAOA+. On 2-regular graphs, the iterations and runs of PQA are respectively 4.13% and 5.4% of the consumption of DS-QAOA+. On 3-regular graphs, the iterations and runs of PQA are respectively 9.09% and 9.1% of the consumption of DS-QAOA+. These results significantly show the efficiency of PQA compared with DS-QAOA+. **That is, PQA can get the quasi-optima in fewer optimization runs and iterations compared with DS-QAOA+, significantly reducing the running costs.**

In addition, we also calculate the total quantum resources consumed by PQA and DS-QAOA+ when they get the quasi-optima on a given graph instance by multiple optimization runs. Specifically, the total resources consumed to find the quasi-optimal solution of the problem are equal to the product of the total number of runs required to find the quasi-optima and the average resource consumption in each run, and more results are shown in Table V. Meanwhile, the mean consumption of PQA and DS-QAOA+ on given graph types is also calculated, showing that the total consumption of qubits and multi-controlled RX gates consumed by PQA is only 1% of that of DS-QAOA+ to get the quasi-optima. By minimizing the quantum resources required while maintaining high performance, PQA becomes increasingly promising for practical implementation in scenarios where resource

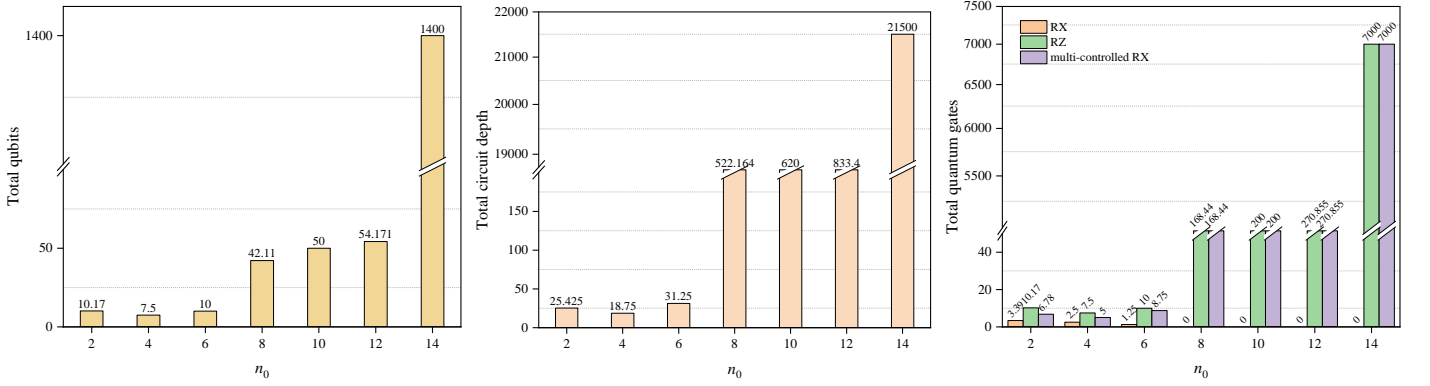


FIG. 10. The total consumption of quantum resources (qubits, circuit depth, and quantum gates) when PQA starts with  $n_0$  and gets the exact MIS solution.

availability is limited.

### C. The comparison of the complexity of obtaining quasi-optimal solution

The above numerical results demonstrate that PQA consumes fewer quantum gates, qubits, and circuit depth, additionally, it requires a smaller total number of iterations to achieve a quasi-optimal solution compared with DS-QAOA+. However, it's worth noting that PQA entails a graph expansion process, which involves classical computations for selecting vertices to be newly added—an aspect absent in DS-QAOA+. Despite the brief duration needed to compute the information utilized in the graph expansion process, we undertake a fair assessment by considering the computational complexity of graph extension. Consequently, this section presents a comprehensive complexity analysis of both PQA and DS-QAOA+.

For PQA, its complexity encompasses the consumption of iterations within the parameter optimization loop as well as the computation involved in the graph expansion process. The external parameter optimization loop necessitates multiple QPU calls to compute the expectation function value during each iteration, a process more intricate than simply determining edge existence between vertices  $v_c$  and  $v_q$ . Here, the complexity of each iteration and each computational step is respectively considered as  $O(t_1)$  and  $O(t_2)$ , and the former is greater than the latter. The computational complexity of PQA to obtain the quasi-optima on graph  $G_i$  is formulated as  $C_{PQA,G_i} = R_{PQA} \times (ITR_{PQA} \times O(t_1) + C_{ex} \times O(t_2))$ , and the computational complexity of DS-QAOA+ is formulated as  $C_{DS,G_i} = R_{DS} \times ITR_{DS} \times O(t_1)$ . Here,  $R_{PQA}$  is the total optimization runs to find the quasi-optima at the required level depth, and  $ITR_{PQA}$  and  $C_{ex}$  are respectively the average consumption of iterations and computation in each run of PQA.

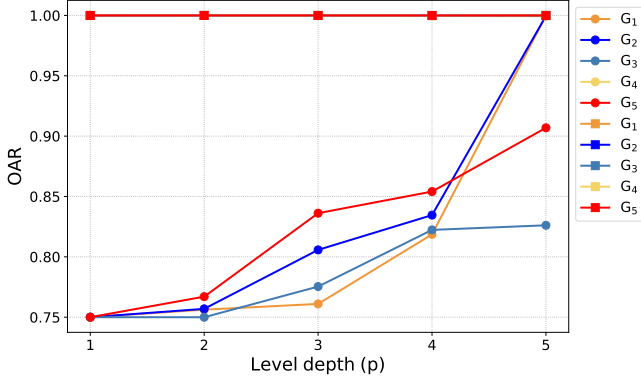
For each graph instance, we independently compute  $C_{PQA,G_i}$  and  $C_{DS,G_i}$ . In the detailed calculations, we

assume  $O(t_1)$  and  $O(t_2)$  to be both equal to  $O(1)$  for simplicity, although this setup somewhat biases the actual complexity against PQA due to the increased complexity of classical calculations. Utilizing this data, we derive the average complexity of PQA (DS-QAOA+) on given graph types. Further elaboration is provided in FIG. 13. These results indicate that the complexity of PQA in achieving quasi-optimal solutions is far less than that required by DS-QAOA+, despite the elevated actual complexity of classical computation. Apart from the above graphs with  $n = 14$ , we additionally analyze the corresponding complexity of PQA and DS-QAOA+ on other ER graphs with varying  $n$ , and more detailed information is provided in Appendix C.

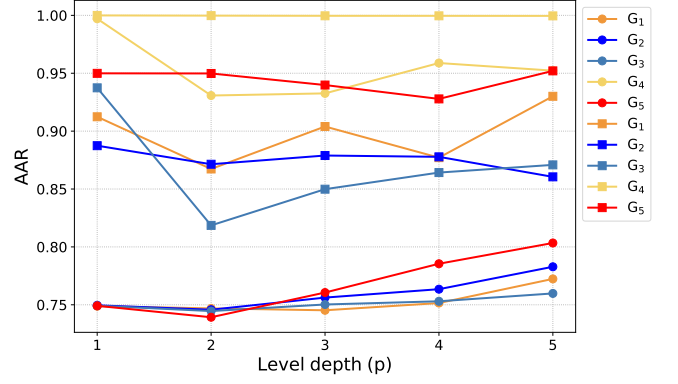
### D. The effect of graph structure on the performance of PQA

In the above simulations, we observe that PQA shows different performance on various graphs, in terms of the average consumption of quantum resources and AAR. To investigate the detailed effect of graph structure on the performance of PQA, we randomly generate 20 ER graphs (with prob = 0.5) for  $n = 8, 9, 10, 11, 12, 13$ , and we execute  $200 \times p$  runs of PQA at each  $p$  when solving the MIS problem on each target graph, where we set  $p = 1$ . We respectively collect the relevant average consumption (including qubits, multi-controlled gates, and the circuit depth) and AAR for each graph at level depth  $p$ . In this paper, we describe the graph structure using  $n$ ,  $m$ , minimal degree, maximal degree, average degree, and the graph density. We record the corresponding features for each graph and visualize the effect of each feature on the performance of PQA when  $p = 1$  in FIG. 14.

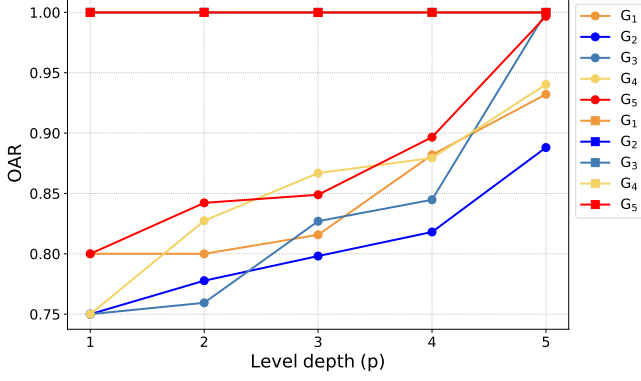
In our data analysis, we utilized Pearson Correlation Coefficient  $R$  ( $\in [-1, 1]$ ) to assess the strength of linear correlation between the given specific graph features and resource consumption (or AAR) when  $p = 1$ . The absolute value of the correlation coefficient indicates the degree of linear correlation, and the two variables are



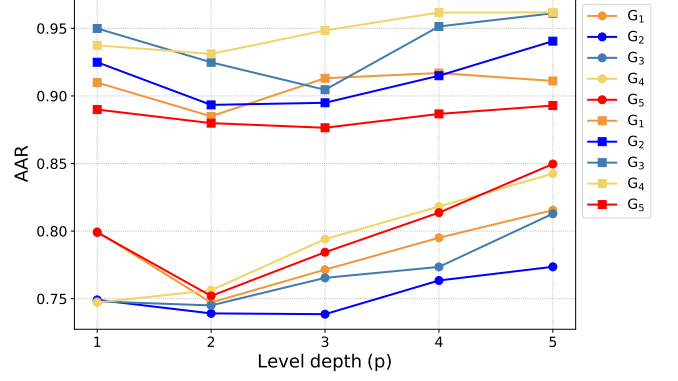
(a)OAR, ER graphs with prob = 0.4



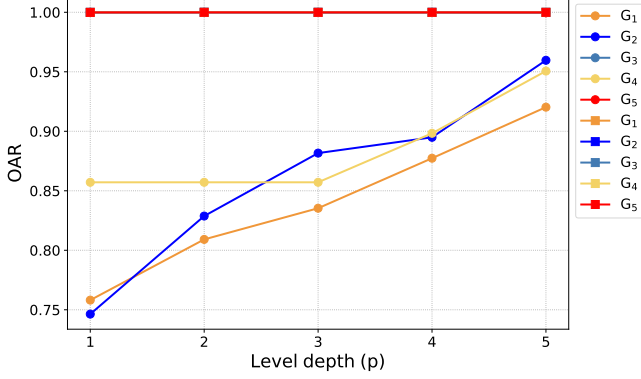
(b)AAR, ER graphs with prob = 0.4



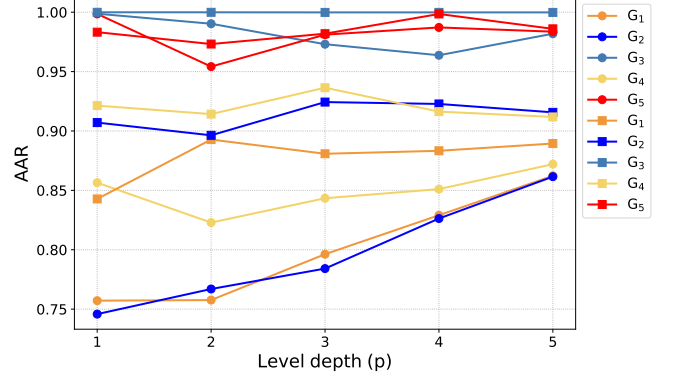
(c)OAR, ER graphs with prob = 0.5



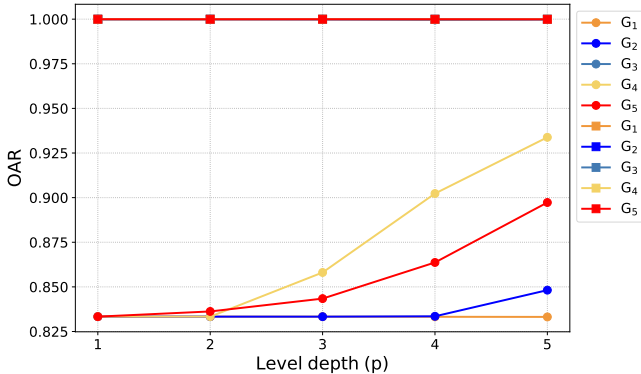
(d)AAR, ER graphs with prob = 0.5



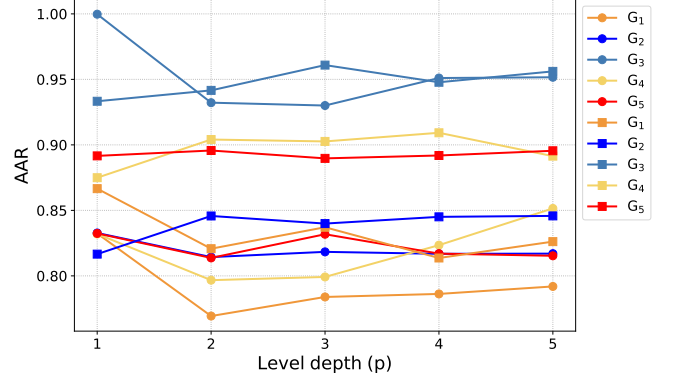
(e)OAR, 2-regular graphs



(f)AAR, 2-regular graphs

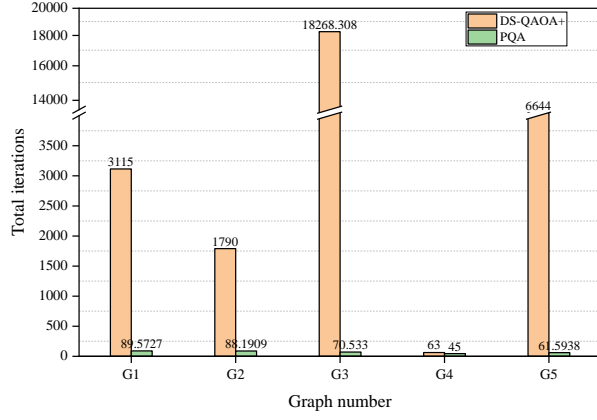


(g)OAR, 3-regular graphs

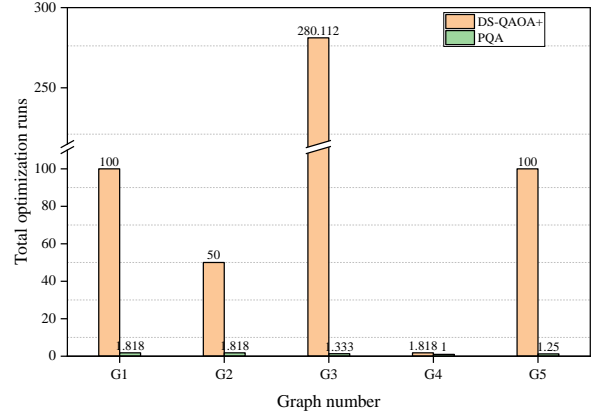


(h)AAR, 3-regular graphs

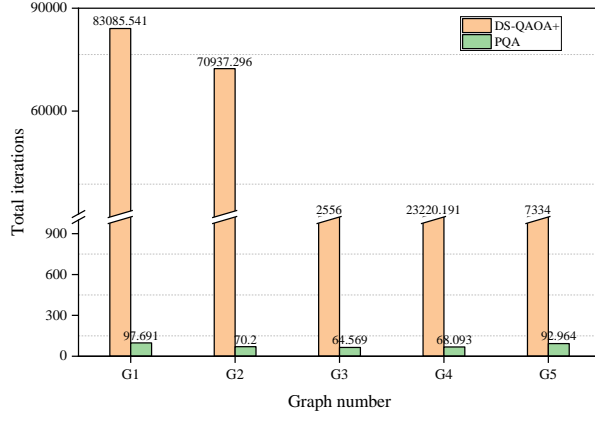
FIG. 11. The AR obtained by PQA and DS-QAOA+ at level depth  $p$  when solving the MIS problem on different graphs with  $n = 14$ . In each subplot, the curve with dots (squares) corresponds to the AR of DS-QAOA+ (PQA). Each curve describes that the AR varies the level depth on a given graph instance. Out of all the graphs tested, PQA can get the exact solution at  $p = 1$ , and the AAR obtained by PQA is higher than DS-QAOA+ on certain graphs at the same level depth.



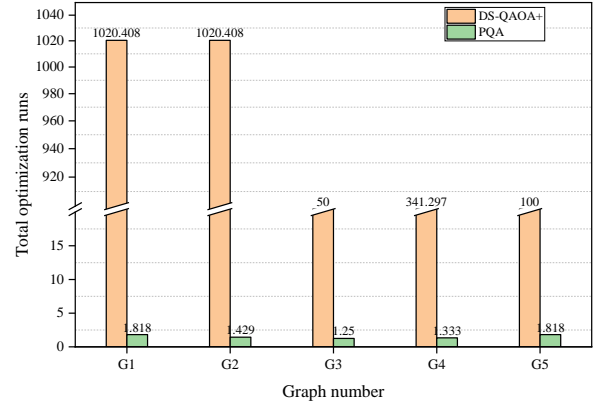
(a) Total iterations, ER graphs, prob = 0.4



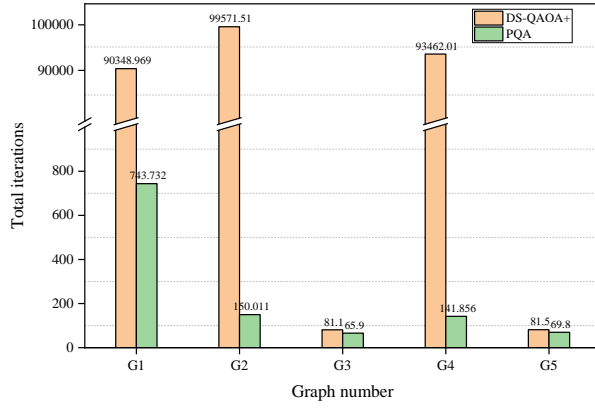
(b) Total optimization runs, prob = 0.4



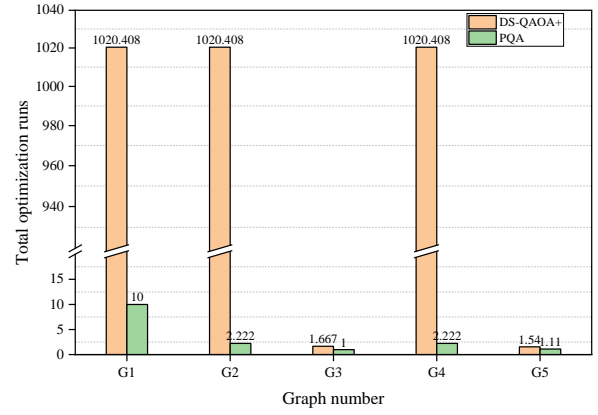
(c) Total iterations, ER graphs, prob = 0.5



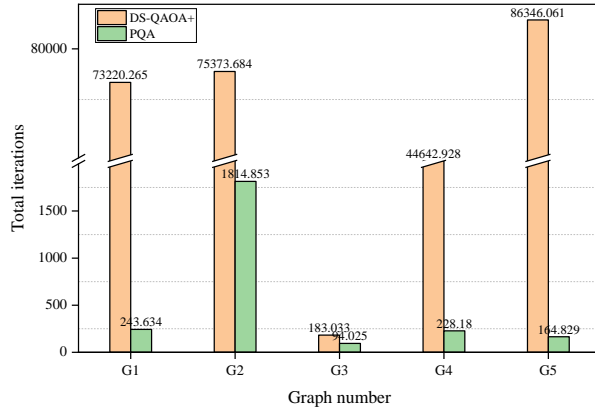
(d) Total optimization runs, prob = 0.5



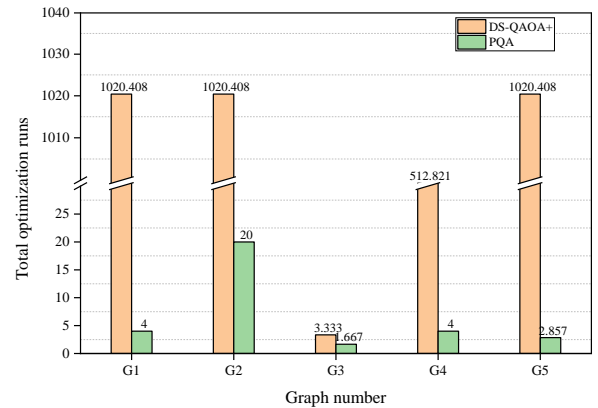
(e) Total iterations, 2-regular graphs



(f) Total optimization runs, 2-regular graphs



(g) Total iterations, 3-regular graphs



(h) Total optimization runs, 3-regular graphs

FIG. 12. The required total iterations and optimization runs when PQA and DS-QAOA+ can get the quasi-optimal solution at their respective required shallowest level depths.

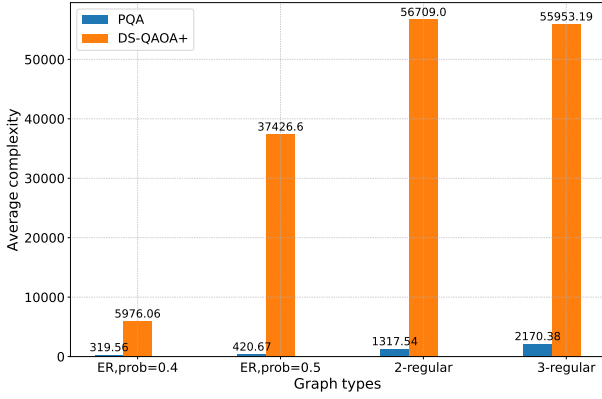


FIG. 13. The average complexity when PQA or DS-QAOA+ finds the quasi-optimal solution on given graph types with  $n = 14$  nodes.

independent of each other if the correlation coefficient is close to 0. Our findings, as depicted in FIG. 14, highlight that the graph density and  $n$  exhibits a stronger correlation with the average consumption of qubits compared with the other features. From our results in FIG. 14, the efficient resource utilization of PQA may be more notable in solving the MIS problem on the graphs with strong connectivity. These investigations contribute to a better understanding of how graph structure influences PQA performance and resource utilization. By identifying key correlations, we can inform the optimization of PQA algorithms for enhanced efficiency and effectiveness in solving CCOPs.

## V. CONCLUSION AND OUTLOOK

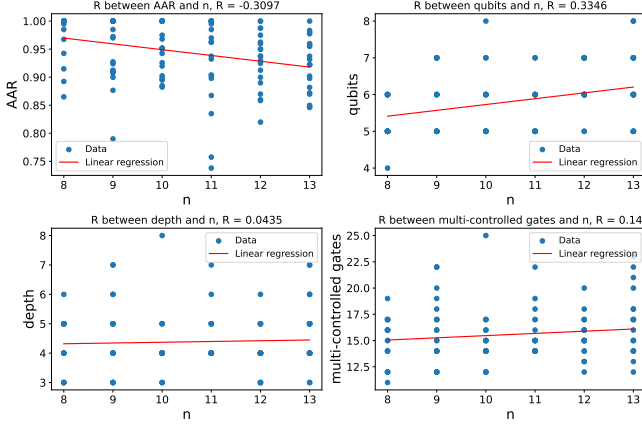
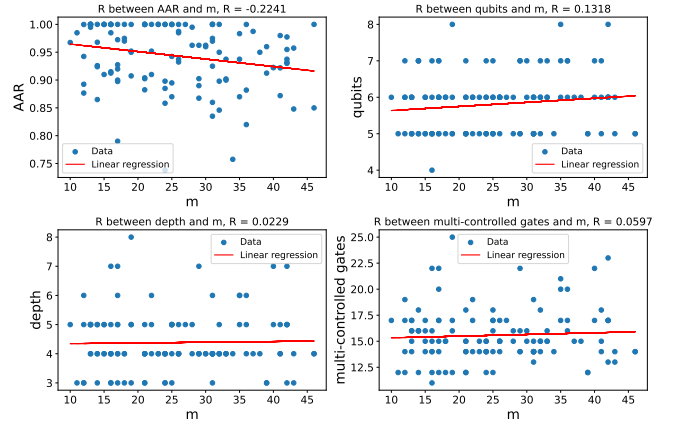
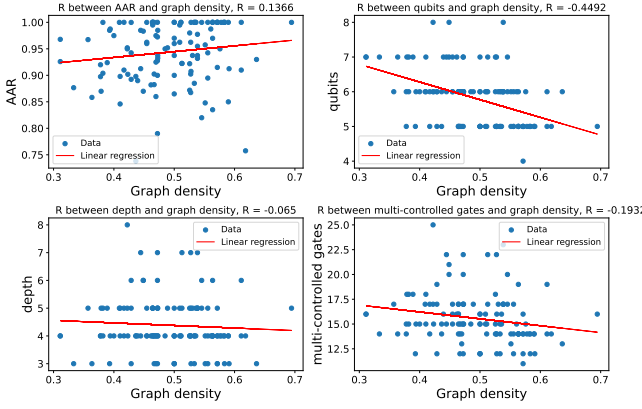
In this paper, we propose a strategy aimed at diminishing the quantum resource consumption during the application of QAOA+ to address the CCOPs, and we take the MIS problem as an example to introduce the idea of PQA and its performance. The central point of PQA is to gradually construct a subgraph that has the same MIS solution as the target graph but has a much smaller graph size. Consequently, solving the MIS problem on this constructed subgraph yields the MIS solution of the target graph. Our simulation results demonstrate that PQA outperforms DS-QAOA+, and the former quantum resources to obtain exact solutions.

The current development of variational quantum algorithms faces significant constraints, primarily due to the limited availability of quantum resources on NISQ devices. These limitations stem from factors such as qubit coherence times and gate error rates, which collectively hinder the scalability and efficiency of quantum algorithms. In light of these challenges, our proposed PQA strategy presents a promising avenue for overcoming limitations and addressing larger-scale problems on NISQ devices. By strategically constructing subgraphs and the early stop mechanisms, PQA offers the potential

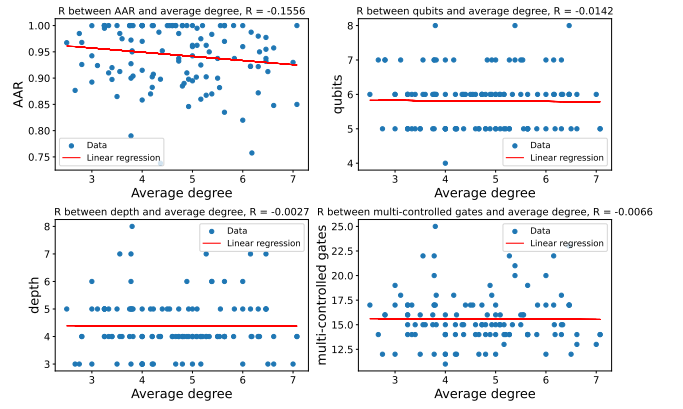
to achieve optimal solutions with reduced resource consumption compared with conventional approaches such as DS-QAOA+. Consequently, leveraging PQA on NISQ devices holds the promise of enabling the solution of more significant and complex optimization problems within the current resource constraints.

In our analysis, we delve into the impact of  $n_0$  (the number of vertices in the initial subgraph) on both the final AR achieved by PQA and the associated consumption of quantum resources. Our findings indicate a potential performance decline for PQA when it starts with a large-scale initial subgraph. For simplicity, PQA initiates with a small-scale subgraph and increments a node during each process of graph extension. However, this incremental expansion approach may inadvertently introduce unnecessary optimization rounds, leading to increased iteration counts. To address this limitation and streamline the optimization process, future research efforts should focus on exploring more effective methods of graph construction and the choice of the initial size  $n_0$  while ensuring PQA performance. One intuitive idea to reduce the number of optimization rounds is adding multiple vertices during each expansion, but it is worth investigating how the performance of PQA changes when multiple vertices are added during each expansion. Another promising avenue is the integration of machine learning techniques, which could optimize the selection of  $n_0$  and dynamically adjust the graph expansion strategy based on real-time feedback. Such advancements hold significant potential for reducing iterations within the external parameter optimization loop, thereby enhancing the overall efficiency and scalability of PQA in tackling quantum optimization problems.

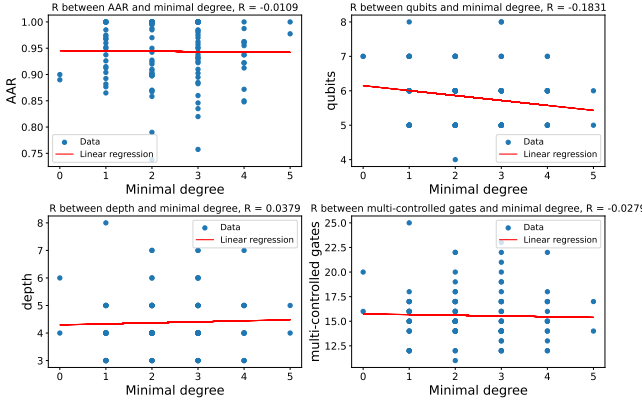
The graph structure also has a significant effect on the performance of PQA. It is also worth designing more refined and efficient graph expansion rules for certain types of graphs to further improve the performance of PQA. While this paper focuses on the MIS problem as an illustrative example, it is crucial to note that the concept of PQA holds potential applicability to a broader spectrum of constrained combinatorial optimization problems. These may include minimum vertex coverage and maximum weighted independent set, among others. In extending the application of PQA to solve these diverse optimization challenges, it becomes imperative to investigate the optimal subgraph construction scale tailored to each specific problem domain. Therefore, future research endeavors should prioritize the systematic exploration of optimal subgraph construction rules for different problem instances. Such investigations are expected to yield valuable insights into fine-tuning the PQA approach for enhanced performance and applicability across various combinatorial optimization domains.

(a) The effect of  $n$  on the average consumption and AAR(b) The effect of  $m$  on the average consumption and AAR

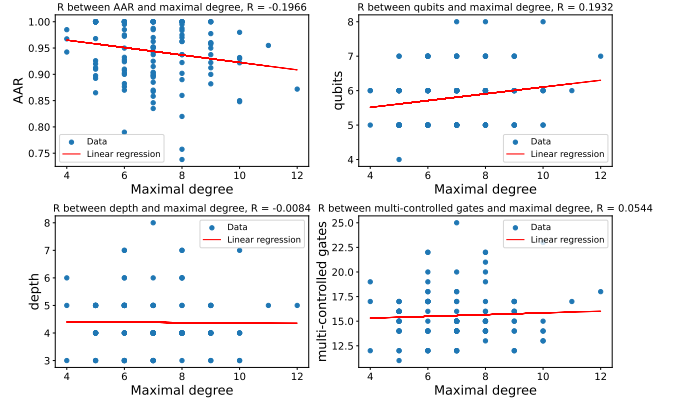
(c) The effect of graph density on the average consumption and AAR



(d) The effect of average degree on the average consumption and AAR



(e) The effect of minimal degree on the average consumption and AAR



(f) The effect of maximal degree on the average consumption and AAR

FIG. 14. The effect of graph structure on the performance of PQA when  $p = 1$ . In each subplot, the slope of linear regression depicts the strength of linear correlation  $R$ , roughly showing the relation between the feature and consumption (or AAR).

## ACKNOWLEDGEMENTS

This work is supported by National Natural Science Foundation of China (Grant Nos. 62371069, 62372048, 62272056), Beijing Natural Science Foundation (Grant No. 4222031) and BUPT Excellent Ph.D. Students Foundation(CX2023123).

- 
- [1] E. Farhi, J. Goldstone, and S. Gutmann, “A quantum approximate optimization algorithm,” (2014), arXiv:1411.4028 [quant-ph].
  - [2] Y. Yu, C. Cao, C. Dewey, X.-B. Wang, N. Shannon, and R. Joynt, *Physical Review Research* **4**, 023249 (2022).
  - [3] B. Zhang, A. Sone, and Q. Zhuang, *npj Quantum Information* **8** (2022).
  - [4] S. Bravyi, A. Kliesch, R. Koenig, and E. Tang, *Physical review letters* **125**, 260505 (2020).
  - [5] R. Herrman, P. C. Lotshaw, J. Ostrowski, T. S. Humble, and G. Siopsis, *Scientific Reports* **12**, 6781 (2022).
  - [6] H. R. Grimsley, S. E. Economou, E. Barnes, and N. J. Mayhall, *Nature communications* **10**, 3007 (2019).
  - [7] H. R. Grimsley, G. S. Barron, E. Barnes, S. E. Economou, and N. J. Mayhall, *npj Quantum Information* **9**, 19 (2023).
  - [8] D. Zhu, N. M. Linke, M. Benedetti, K. A. Landsman, N. H. Nguyen, C. H. Alderete, A. Perdomo-Ortiz, N. Korda, A. Garfoot, C. Brecque, *et al.*, *Science advances* **5**, eaaw9918 (2019).
  - [9] Y. Du, T. Huang, S. You, M.-H. Hsieh, and D. Tao, *npj Quantum Information* **8**, 62 (2022).
  - [10] H. L. Tang, V. Shkolnikov, G. S. Barron, H. R. Grimsley, N. J. Mayhall, E. Barnes, and S. E. Economou, *PRX Quantum* **2**, 020310 (2021).
  - [11] C. Bravo-Prieto, R. LaRose, M. Cerezo, Y. Subasi, L. Cincio, and P. J. Coles, *Quantum* **7**, 1188 (2023).
  - [12] X. Wang, Z. Song, and Y. Wang, *Quantum* **5**, 483 (2021).
  - [13] Y. Song, Y. Wu, S. Wu, D. Li, Q. Wen, S. Qin, and F. Gao, *Science China Physics, Mechanics & Astronomy* **67**, 250311 (2024).
  - [14] J. Preskill, *Quantum* **2**, 79 (2018).
  - [15] M. Cerezo, A. Arrasmith, R. Babbush, S. C. Benjamin, S. Endo, K. Fujii, J. R. McClean, K. Mitarai, X. Yuan, L. Cincio, and P. J. Coles, *Nature Reviews Physics* **3**, 625 (2021).
  - [16] K. Bharti, A. Cervera-Lierta, T. H. Kyaw, T. Haug, S. Alperin-Lea, A. Anand, M. Degroote, H. Heimonen, J. S. Kottmann, T. Menke, *et al.*, *Reviews of Modern Physics* **94**, 015004 (2022).
  - [17] M. Streif and M. Leib, *Quantum Science and Technology* **5**, 034008 (2020).
  - [18] L. Zhou, S.-T. Wang, S. Choi, H. Pichler, and M. D. Lukin, *Phys. Rev. X* **10**, 021067 (2020).
  - [19] S. H. Sack and M. Serbyn, *Quantum* **5**, 491 (2021).
  - [20] F. G. S. L. Brandao, M. Broughton, E. Farhi, S. Gutmann, and H. Neven, “For fixed control parameters the quantum approximate optimization algorithm’s objective function value concentrates for typical instances,” (2018), arXiv:1812.04170 [quant-ph].
  - [21] J. Wurtz and D. Lykov, *Phys. Rev. A* **104**, 052419 (2021).
  - [22] M. Alam, A. Ash-Saki, and S. Ghosh, in *2020 Design, Automation & Test in Europe Conference & Exhibition (DATE)* (IEEE, 2020) pp. 686–689.
  - [23] S. H. Sack, R. A. Medina, R. Kueng, and M. Serbyn, *Physical Review A* **107**, 062404 (2023).
  - [24] V. Akshay, D. Rabinovich, E. Campos, and J. Biamonte, *Phys. Rev. A* **104**, L010401 (2021).
  - [25] C. Moussa, H. Wang, T. Bäck, and V. Dunjko, *EPJ Quantum Technology* **9** (2022).
  - [26] X.-H. Ni, B.-B. Cai, H.-L. Liu, S.-J. Qin, F. Gao, and Q.-Y. Wen, “Multilevel leapfrogging initialization for quantum approximate optimization algorithm,” (2024), arXiv:2306.06986 [quant-ph].
  - [27] L. Zhu, H. L. Tang, G. S. Barron, F. A. Calderon-Vargas, N. J. Mayhall, E. Barnes, and S. E. Economou, *Phys. Rev. Res.* **4**, 033029 (2022).
  - [28] S. Hadfield, Z. Wang, B. O’gorman, E. G. Rieffel, D. Venturelli, and R. Biswas, *Algorithms* **12**, 34 (2019).
  - [29] Y. Chai, Y.-J. Han, Y.-C. Wu, Y. Li, M. Dou, and G.-P. Guo, *Physical Review A* **105**, 042415 (2022).
  - [30] S. Khairy, R. Shaydulin, L. Cincio, Y. Alexeev, and P. Balaprakash, *Proceedings of the AAAI Conference on Artificial Intelligence* **34**, 2367 (2020).
  - [31] M. M. Wauters, E. Panizon, G. B. Mbeng, and G. E. Santoro, *Physical Review Research* **2** (2020).
  - [32] Y. Pan, Y. Tong, and Y. Yang, *Physical Review A* **105**, 032433 (2022).
  - [33] L. Li, J. Li, Y. Song, S. Qin, Q. Wen, and F. Gao, arXiv preprint arXiv:2311.02302 (2023).
  - [34] S. Brandhofer, D. Braun, V. Dehn, G. Hellstern, M. Hüls, Y. Ji, I. Polian, A. S. Bhatia, and T. Wellens, *Quantum Information Processing* **22**, 25 (2022).
  - [35] Y. Zhang, X. Mu, X. Liu, X. Wang, X. Zhang, K. Li, T. Wu, D. Zhao, and C. Dong, *Applied Soft Computing* **118**, 108554 (2022).
  - [36] P. Vikstål, M. Grönkvist, M. Svensson, M. Andersson, G. Johansson, and G. Ferrini, *Phys. Rev. Appl.* **14**, 034009 (2020).
  - [37] J. Wurtz and P. Love, *Phys. Rev. A* **103**, 042612 (2021).
  - [38] Y. Chatterjee, E. Bourreau, and M. J. Rančić, arXiv preprint arXiv:2301.06978 (2023).
  - [39] Y. Ruan, Z. Yuan, X. Xue, and Z. Liu, *Information Sciences* **619**, 98 (2023).
  - [40] R. M. Karp, *50 Years of Integer Programming* (2010).
  - [41] J. R. Finžgar, A. Kerschbaumer, M. J. Schuetz, C. B. Mendl, and H. G. Katzgraber, arXiv preprint arXiv:2308.13607 (2023).
  - [42] Z. H. Saleem, T. Tomesh, B. Tariq, and M. Suchara, *SN Computer Science* **4**, 183 (2023).
  - [43] S. Hadfield, Z. Wang, E. G. Rieffel, B. O’Gorman, D. Venturelli, and R. Biswas, in *Proceedings of the Second International Workshop on Post Moores Era Supercomputing* (2017) pp. 15–21.
  - [44] Z. H. Saleem, *International Journal of Quantum Information* **18**, 2050011 (2020).
  - [45] S.-S. Wang, H.-L. Liu, Y.-Q. Song, F. Gao, S.-J. Qin, and Q.-Y. Wen, *Physica A: Statistical Mechanics and its Applications* **626**, 129089 (2023).
  - [46] J. Cook, S. Eidenbenz, and A. Bäertschi, in *2020 IEEE International Conference on Quantum Computing and Engineering (QCE)* (IEEE, 2020) pp. 83–92.
  - [47] Z. Wang, N. C. Rubin, J. M. Dominy, and E. G. Rieffel, *Physical Review A* **101**, 012320 (2020).
  - [48] Z. He, R. Shaydulin, S. Chakrabarti, D. Herman, C. Li, Y. Sun, and M. Pistoia, arXiv preprint arXiv:2305.03857 (2023).
  - [49] T. Tomesh, N. Allen, and Z. Saleem, arXiv preprint arXiv:2210.04378 (2022).
  - [50] L. T. Brady and S. Hadfield, arXiv preprint arXiv:2309.13110 (2023).

- [51] T. Tomesh, Z. H. Saleem, M. A. Perlin, P. Gokhale, M. Suchara, and M. Martonosi, in *2023 IEEE International Conference on Quantum Computing and Engineering (QCE)*, Vol. 1 (IEEE, 2023) pp. 1–12.
- [52] T. Peng, A. W. Harrow, M. Ozols, and X. Wu, *Physical review letters* **125**, 150504 (2020).
- [53] A. Galda, X. Liu, D. Lykov, Y. Alexeev, and I. Safro, in *2021 IEEE International Conference on Quantum Computing and Engineering (QCE)* (IEEE, 2021) pp. 171–180.
- [54] R. Shaydulin, P. C. Lotshaw, J. Larson, J. Ostrowski, and T. S. Humble, *ACM Transactions on Quantum Computing* **4**, 1 (2023).
- [55] J. A. Montanez-Barrera, D. Willsch, and K. Michielsen, “Transfer learning of optimal qaoa parameters in combinatorial optimization,” (2024), arXiv:2402.05549 [quant-ph].
- [56] A. Lucas, *Frontiers in physics* **2**, 5 (2014).
- [57] T. Albash and D. A. Lidar, *Rev. Mod. Phys.* **90**, 015002 (2018).
- [58] M. Halldórsson and J. Radhakrishnan, in *Proceedings of the twenty-sixth annual ACM symposium on Theory of computing* (1994) pp. 439–448.
- [59] R. Shaydulin, I. Safro, and J. Larson, in *2019 IEEE High Performance Extreme Computing Conference (HPEC)* (2019) pp. 1–8.

## Appendix A: The extension of the subgraph

In this section, we introduce the process of the graph extension based on two various derived subgraphs. Denote the current subgraph as  $G_i = (V_i, E_i)$ . For the first subgraph in FIG. A1,  $V_i = \{0, 1, 2\}$  and  $E_i = \{(0, 1), (0, 2)\}$ . Thus, the candidate vertex set  $V_C = V - V_i = \{3, 4\}$ . Our task is to choose the node from  $V_C$  that has the lowest connection with the current subgraph as the next vertex to be added to the subgraph  $G_i$ . If the node 3 is added to  $G_i$ , the corresponding  $C(v_c = 3) = 1$ . Otherwise, the node 4 is added to  $G_i$ , and  $C(v_c = 4) = 1$ . Nodes 3 and 4 both have the lowest connection with the current subgraph, and we conduct the next round of selection. If the node 3 is added to  $V_i$ , the edge  $(0, 3)$  should be added to  $E_i$ . At this time,  $V_C = \{4\}$ , and  $C(v_c = 4) = 2$ . Similarly, we calculate  $C(v_c = 3) = 2$  if  $V_C = \{3\}$ . After two rounds of calculation, nodes 3 and 4 both satisfy our selection rule, and we can randomly choose one into  $V_i$ . If the node 3 (4) is added to  $V_i$ , the edge  $(0, 3)$  ( $(0, 4)$ ) is added to  $E_i$ . The newly constructed subgraph is  $G_{i+1} = \{\{0, 1, 2, 3\}, \{(0, 1), (0, 2), (0, 3)\}\}$  (or  $G_{i+1} = \{\{0, 1, 2, 4\}, \{(0, 1), (0, 2), (0, 4)\}\}$ ).

While for the second subgraph in FIG. A1,  $V_i = \{0, 1, 3\}$  and  $E_i = \{(0, 1), (0, 3)\}$ . The candidate vertex set  $V_C = \{2, 4\}$ , and we get  $C(v_c = 2) = 1$  and  $C(v_c = 4) = 2$ . We prefer to opt for the node with a minimal value of  $C(v_c)$  from the candidate vertex set. Thus, node 2 is the next node to be added to  $V_i$ . At this time, the edge  $(0, 2)$  is added to  $E_i$ . The newly constructed subgraph is  $G_{i+1} = \{\{0, 1, 2, 3\}, \{(0, 1), (0, 2), (0, 3)\}\}$ .

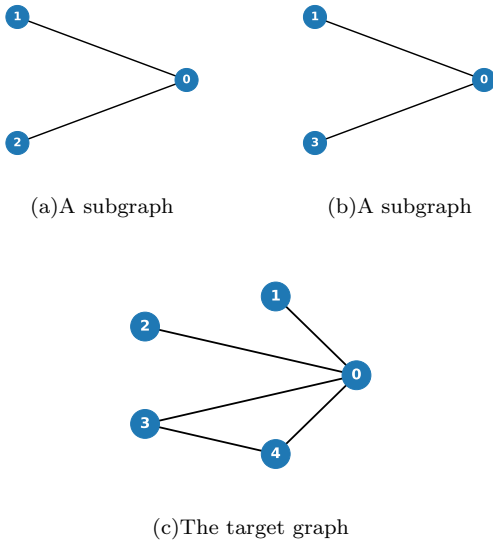


FIG. A1. The target graph and its induced subgraphs.

## Appendix B: The changes of expectation function values in an optimization run of PQA

In our simulations, we adopt PQA to solve the MIS problem on an ER graph with  $n = 14$ , and we set the level depth  $p = 4, 5$ . There are  $20 \times p$  optimization runs of PQA at each level depth. In this section, we give the detailed changes of the expectation function value in each optimization run of PQA. From the simulation results in FIG. A2, we observe that the vibration of the expectation function values may postpone the termination of PQA. At this time, the final induced subgraph may achieve the same graph size as the target graph when an optimization run of PQA stops. In addition, the results demonstrate that PQA also reaches the termination condition even though the current subgraph has a smaller independence number than the target graph, such as the steady phase (the corresponding expectation function value is 3).

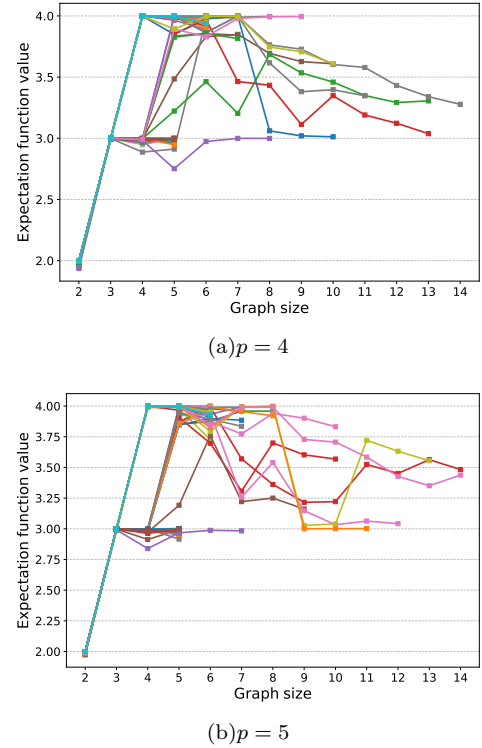


FIG. A2. The changes of expectation function values in an optimization run of PQA at level depth  $p$ , where  $n_0 = 2$  and the maximal expectation function value is 4. In each subplot, there are  $20 \times p$  runs of PQA, and each curve corresponds to an optimization run of PQA, where the square on each curve is the obtained function value after each optimization round. The Y-axis represents the number of nodes in the current induced subgraph, where the maximal value of the Y-axis reflects the maximal size of the final subgraph when PQA terminates. These figures suggest more optimization rounds are required in an optimization run when the expectation function values obviously fluctuate back and forth (i.e., the values do not meet the stop condition).

### Appendix C: The complexity of PQA and DS-QAOA+ on ER graphs with various $n$

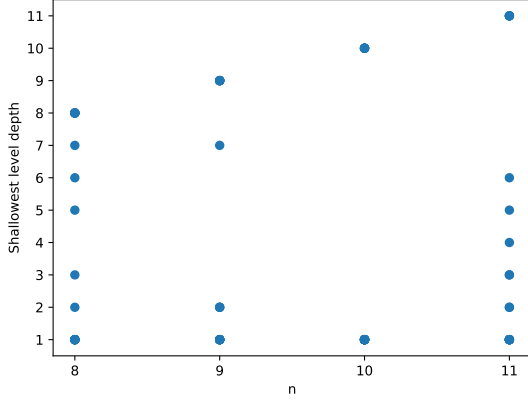


FIG. A3. The required shallowest level depth for DS-QAOA+ to obtain the quasi-optima on various ER graphs with different vertex numbers.

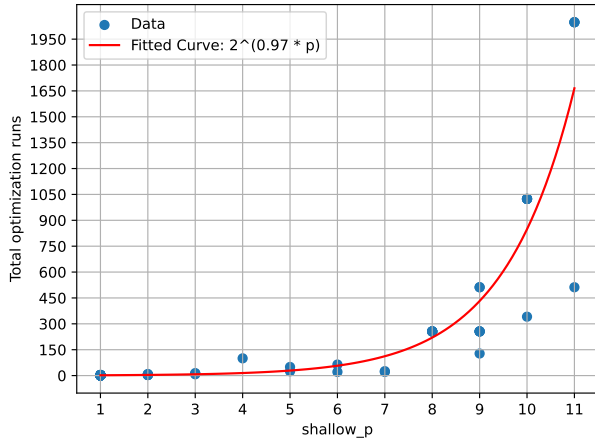


FIG. A4. The total number of optimization runs at the corresponding shallowest level depth for DS-QAOA+ to attain the quasi-optima, where the red curve is fitted by these blue dots (simulation results).

To investigate the complexity of PQA and DS-QAOA+ on other graphs with various  $n$ , we set  $n = 8, 9, 10, 11$  and randomly generate 20 ER graphs with prob = 0.5 for each  $n$ . On each graph instance, we execute multiple runs of PQA as well as DS-QAOA+ to find the optimal

or quasi-optimal solution of the problem. In the specific solution of each graph, we set the level depth  $p$  from 1 to  $n$ . When the level depth is less than or equal to 5, 100 optimization runs are executed under each level depth. Otherwise,  $2^p$  optimization runs are executed. We independently count the quasi-optima that can be obtained by PQA and DS-QAOA+ in all optimization runs, and the resource consumption in terms of the shallowest level depth, the number of optimization runs, and the number of iterations required to obtain the quasi-optimal solution of the problem. The numerical results show that PQA is able to obtain the quasi-optima at  $p = 1$  on the randomly given graph instances, while DS-QAOA+ requires more level depths, such as shown in FIG. A3. More importantly, PQA tends to require polynomial number of optimization runs to obtain the quasi-optimal solution of the problem at the shallowest level depth, whereas DS-QAOA+ tends to require an exponential number of optimization runs to obtain a similar performance (but inferior to PQA), such as shown in FIG. A4. Based on the statistically obtained data, we computed the average complexity  $C_{avg, PQA} = \frac{\sum_{i=1}^{i=20} C_{PQA, G_i}}{20}$  needed to solve the MIS problem on the  $n$ -vertex graph and obtain the quasi-optimal solution of the problem, respectively, and the specific results are shown in FIG. A5. For PQA, its complexity of finding the quasi-optima is much less than that of DS-QAOA+.

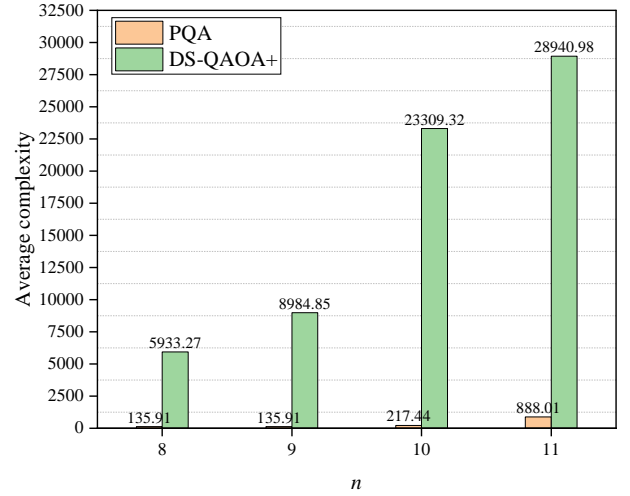


FIG. A5. The average complexity when PQA or DS-QAOA+ finds the quasi-optimal solution on ER graphs with  $n$  nodes.